ORE TEXTURE MEASURMENT USING INFRARED HYPERSPECTRAL IMAGERY OF PORPHYRY CU PEBBLES FOR COPPER CONTENT ESTIMATION

MOCHAMAD RIFAT NOOR
FEBRUARY, 2019

SUPERVISORS:

Dr. F.J.A. (Frank) van Ruitenbeek
Dr. H.M.A. (Harald) van der Werff

Ore Texture Measurement Using Infrared Hyperspectral Imagery of Porphyry Cu Pebbles for Copper Content Estimation

MOCHAMAD RIFAT NOOR

Enschede, The Netherlands, FEBRUARY, 2019

Thesis submitted to the Faculty of Geo-Information Science and Earth Observation of the University of Twente in partial fulfilment of the requirements for the degree of Master of Science in Geo-information Science and Earth Observation.
Specialization: Applied Earth Sciences

SUPERVISORS:
Dr. F.J.A. (Frank) van Ruitenbeek
Dr. H.M.A. (Harald) van der Werff

THESIS ASSESSMENT BOARD:
Prof. Dr. F.D. van der Meer
Dr. Mike Buxton (Technical University Delft)

ABSTRACT

Ore textures provide valuable information on mineral deposition and development. Traditionally, ore texture is identified using visual interpretation on the rock sample and thin section analysis of rock sample using microscopy. This research was conducted to investigates the ore texture using high-resolution hyperspectral imagery in SWIR range which associated with the copper content. The hyperspectral images of milled pebbled rock were pre-processed using ENVI and HyPpy software package. The mineral maps were generated from the decision tree classification. The mineral that presents in milled pebbles rock samples were illite, muscovite, tourmaline, chlorite, and kaolinite. The mineral map expressed mineral distribution spatially and illustrate the texture of the rock sample. The mineral map was measured by Shaper script from IDL. Several parameters were produced from the Shaper script software, such as convexity, and compactness. The rock measurement generated several parameters including flattening, standardize resultant and relative object size. The rock containing tourmaline has a high content of copper than rock not containing tourmaline. Based on the statistic result, flattening and convexity of tourmaline show low correlation with the copper grade. The relative object which illustrate distribution of clast and orientation of clast has low correlation with the copper content. However, the parameter above can be used to highlight high copper content in the rock samples.

Keywords: Ore texture, hyperspectral image, mineral map, copper content

ACKNOWLEDGEMENTS

TABLE OF CONTENTS

LIST OF FIGURES

LIST OF TABLES

1.   INTRODUCTION

Porphyry deposit is the largest source of copper, they commonly form in/near subduction zones and associated with magmatic arcs (Pirajno, 2009). The deployment of this deposit type is extensive in America, Europe, Asia and Australia (Northey et al., 2017). Porphyry deposit is the result of hydrothermal systems (Arndt et al., 2012). There are four types of hydrothermal systems that could be differentiated based on the solution mixture of the hydrothermal fluids, namely: 1) epithermal and porphyry system that formed when the hydrothermal fluid interacts with meteoric water, 2) volcanic massive sulfide (VMS) system which is produced when the hydrothermal fluid is associated with sea water, 3) sedimentary exhalative deposits (SEDEX) system that is produced from the contact of the hydrothermal fluid with basinal water, and 4) orogenic Au that is generated due to fluids interaction with metamorphic rocks during orogenic events (Arndt et al., 2012).

Porphyry deposits are affected by the intrusion of subvolcanic rocks from several episodes of intrusion. These intrusions bring metal-bearing magmatic solutions that mix with meteoric water. They generate mineralization of ores which located about 1 km beneath the earth's surface (Corbett et al., 1998). Hydrothermal systems develop several alteration zones; such as phyllic, propylitic, argillic, potassic, advanced argillic, and silicic (Yousefia et al., 2018). The propylitic zone is located in the outer region of the hydrothermal system. Typically, this zone has broad coverage and indicated by the occurrence of carbonate, epidote, and chlorite. Argillic alteration zone is characterized by clay minerals such as illite, smectite, and kaolinite. Closer to the alteration source is a phyllic zone, which is indicated by sericite, quartz, and pyrite. This zone has been known as a host of the highest ore concentration. Potassic alteration is located in the inner zone that comprises of biotite, magnetite, anhydrite, and rutile (Sillitoe, 2010).

Porphyry deposits have distinctive ore and texture characteristics such as mineral replacement, wall rock alteration and metasomatism (Taylor, 2009). These are yielded from the interaction between hydrothermal fluids with the host rock (Robb, 2005). The hydrothermal fluid is commonly percolated through rocks by their pore spaces or fractures as a primary and secondary permeability, respectively. Ineson, (1989) also described that disseminated and stockwork texture occurs in the porphyry system. Disseminated texture usually has ore mineral scattered along fractures within the rock. Meanwhile, stockwork is formed by some veinlet which is connected (Allaby, 2013).

Craig & Vaughan (1994) explained that ore texture has an intergranular relationship. Ore texture in porphyry system is formed by a hydrothermal fluid (Robb, 2005). It can assist in the interpretation of the ore deposit forming process such as weathering, oxidation, re-equilibration, metamorphism, annealing, and cementation (Ineson, 1989). Ore texture can be measured based on some parameters such as size, shape, orientation, position, and interconnection of grain/crystals. These parameters can be analyzed using conventional or advanced techniques; for instance, the petrological method using a polarizing microscope has been used for such long times to study the ore texture distribution. Nowadays, more advanced techniques such as cathodoluminescence, scanning electron microscopy (SEM), transmission electron microscopy (TEM), and electron microprobe (EMP) can be used to quantitative estimate the textural properties of ore deposit (Higgins, 2006). The hyperspectral image which resulted from hyperspectral camera also can be used for ore texture identification.

The hyperspectral imaging tools have been used to analyze chip rock and/or drill core in SWIR wavelength. Clark et al. (1990) have been use high spectral resolution reflectance spectroscopy to differentiate minerals and determine their elemental composition. Dalm et al., (2017) distinguished ore and waste material by integrating the crystallinity and mineral map, with geochemical data. (Mathieu et al., (2017) identified alteration minerals and rock textures such as veins, bedding, and foliation on a drill core sample from Uranium deposit using SWIR imagery. (Laakso et al., (2018) investigated the phosphorus mineral from carbonate rock using the visible near-infrared (VNIR) and shortwave infrared (SWIR) hyperspectral images and performed a validation based on a Mineral Liberation Analyzer. Tripathy et al, (2017) differentiated gangue mineral and

ore using multispectral imagery with color texture approach. Barrie et al., (2010) observed textural variation such as orientation, grain size, and composition to identify pyrite deformation.

In this study, the hyperspectral image will be used to create a mineral map. The geometrical parameter will be extracted from the mineral map to estimate copper grade in porphyry samples using the SWIR range of a high-resolution multispectral laboratory tool SisuCHEMA.

1.1. Problem statement

Ore texture provides valuable information on mineral deposition and their development processes. In the past, ore texture identification was done by direct visual observation on the rock samples and thin section analysis of rock sample using microscopy. However, quantitative information of ore texture is difficult to obtain by the aforementioned interpretation. Also, the relationship between ore texture and metal content, especially copper is not yet available. Therefore, it is important to find the correlation between the ore texture and the mineralogy information.

This research is conducted to find the correlation between ore texture and copper content, specifically. Instead of RGB photo rock samples, hyperspectral images will be used to determine the ore texture. Hyperspectral images obtained from the infrared camera will be used for mineral mapping to locate the mineral distribution spatially. Mineral distribution which is correlated with ore texture will be used for copper content estimation. The image will be processed by Shaper software to obtain several shape parameters such as basic shape, variation shape and size, size distribution and object orientation. This result will assist in the prediction of copper content using statistical techniques.

1.2. Objectives and research questions

1.2.1. Main objective

This research aims to analyze and measure ore texture in porphyry Cu milled pebbles sample using high-resolution hyperspectral images in the shortwave infrared (SWIR) wavelength range to enhance prediction of a copper content.

1.2.2. Specific objectives
1. To identify ore textures visually from porphyry copper deposit using RGB photos
2. To create mineral maps that show distribution and abundance of alteration mineral in a sample using high-resolution hyperspectral images.
3. To analyze and measure ore textures parameter from SWIR hyperspectral image identification
4. To assess the relationship between copper content with ore texture parameter

1.2.3. Research question
1. What kind of textures can be determined by visual interpretation?
2. What kind of minerals can be detected in the SWIR wavelength range?
3. What kind of texture can be determined from hyperspectral imagery?
4. What is the relationship between copper content with ore texture measurement?

1.3. Hypothesis

Los bronces porphyry deposit is dominated by breccia rock with some texture, such as stockworks, veinlets and disseminated. However, Donoso breccia is the primary source of the highest primary copper mineralization in the deposit. The mineralization occurs primarily in breccia matrix and appears as coarse aggregates or irregular spots of bornite, pyrite, and chalcopyrite.

1.4.   Scope and limitation

The forty-three pebbles samples used in this research were obtained from the Los Bronces mine which is operated by Anglo American. The pebbles were originated from mill ore rock that contained copper which were left uncrushed after mine operation. In the standard mine operation, these pebbles will be separated from ore and will be stored as waste. However, these milled pebbles still contain economical concentration. The hyperspectral images of pebbles were scanned and analyzed which focused on white mica mineral mapping by the previous researcher, Ms. Agus.

1.5.   Thesis structure

This thesis is divided into six chapters:
Chapter 1: Introduction
Chapter 2: Research background
Chapter 3: Methodology
Chapter 4: Result
Chapter 5: Discussion and conclusion

2. RESEARCH BACKGROUND

2.1. Geology setting

The study area is located at Los Bronces mine in Andes Highland with altitude from 2700 to 4100 m, Central Chile (Frikken et al., 2005) Los Bronces is porphyry Copper-Molybdenum (Cu-Mo) type deposit that contains disseminated and stockworks copper-iron-molybdenum sulfide mineralization which formed between 4.9 m.y. And 7.9 m.y. Ago. This deposit is associated with hydrothermal tourmaline-cemented breccia (Warnaars et al., 1985).

The Los Bronces porphyry Cu deposit is operated by Anglo American Sur. Los Bronces porphyry consisted of several episodes of mineralized hydrothermal breccia complexes dated at 7.3 to 4.2 Ma (Frikken et al., 2005) and intruded the older porphyry Cu deposit (Warnaars et al., 1985). It emerges on the western side of the San Francisco batholith, and intrudes in two periods, first during the Paleocene-Oligocene and the second during Miocene (Warnaars et al., 1985). The deposit is hosted by Miocene volcanic and volcanoclastic rocks of Farrelones formation and Abanico Formation (Warnaars et al., 1985). In the late Miocene, the San Francisco batholith is intruded by the volcanic rock, then Los Bronces deposit appeared and was overlain by Miocene volcanic, the Farellones Formation. In the second episode, the Farellones Formation and the San Francisco batholith were intruded by late mineral felsic porphyries and mineralized biotite-tourmaline-cemented breccias. The ore zones have NNW trending and appear within and below a ~1.75 km wide.

Tourmaline-cemented breccias are the host of mineralization (Warnaars et al., 1985). Seven types of tourmaline breccia were identified as copper bearing. This breccia has 2 km long and 0.7 wide. The various breccias are characterized by their locations, matrix, clasts, shapes types and degrees of mineralization, and alteration. The breccias are usually monolithic but in some case are bi-lithic or hetero lithic with most clasts consisting of quartz monzonite or andesite with locally minor amounts of quartz latite porphyry, monzodiorite and vein quartz. The breccia matrices consist of variable amounts of quartz, tourmaline, specularite, anhydrite, pyrite, chalcopyrite, bornite, molybdenite, sericite, chlorite, and rock flour.

The hydrothermal processes of Los Bronces porphyry began during the late Miocene, with a large area of alteration. The hydrothermal process was characterized by actinolite-magnetite mineral, with brecciated and veins texture. Cu concentration appears in intense potassic alteration zone and characterized by secondary biotite with breccia-matrix, stockwork, and disseminated texture. A subsequent event occurred where breccia rock was formed which was characterized by younger tourmaline-rich breccia pipes. The tourmaline breccias clast were sericitised during the brecciated process, in the earlier potassic alteration.

2.2. Rock texture

Rock texture is an arrangement of grain, glass, and crystal (Higgins, 2006). Craig et al., (1994) explain that ore texture has an intergranular relationship. Ore texture in porphyry system is formed by a hydrothermal fluid (Robb, 2005). It can assist in the interpretation of the ore deposit forming process such as weathering, oxidation, re-equilibration, metamorphism, annealing, and cementation (Ineson, 1989). The postdepositional and origin of ore can be identified using rock texture. Texture and mineral composition can contribute depositional condition of sedimentary rock, sedimentary rock provenance, crystallization and mixing magma for igneous rock, metamorphic process and formation of metamorphic rock. Alteration texture can provide information on alteration intensity process (Taylor, 2009).

Ore texture can be measured based on some parameters such as size, shape, orientation, position, and interconnection of grain/crystals. These parameters can be analyzed using conventional or advanced techniques.

The object shape parameter is divided into three parameters; there are object area, compactness, and convexity (van Ruitenbeek et al., 2019). The object area is the amount of pixel in one object. The compactness of the object is described in the equation below.

$$Compactness = 4\pi \frac{object\ area}{object\ perimeter^2}$$

The convexity is expressed by convex hull parameter divided perimeter. The purely convex shape has value 1. Orientation and diameter of the object can be obtained using fitted ellipses. The major and minor axis from the center position of ellipse can be used to determine flattening of the object. The flattening can be calculated by equation:

$$\text{Flattening} = \frac{\text{Length minor axis}}{\text{Length major axis}}$$

Hollowness object can be identified by equation:

$$\text{Hollowness} = \frac{\text{Object area}}{\text{Convex hull area}}$$

The direction of the image object is calculated using an orientation angle of the image. Resultant vector was measured from each object orientation. The resultant vector is defined as

$$R = \sqrt{(X_r^2 + Y_r^2)}$$

The standardized resultant is calculated to standardize all resultant length object.
The mean direction of the vector resultant was the angular average of all object orientation vectors in an image:

$$\bar{\theta} = \tan^{-1}\left(\frac{X_r}{Y_r}\right)$$

The mean direction is illustrated using a rose diagram and produced with Stereonet software.
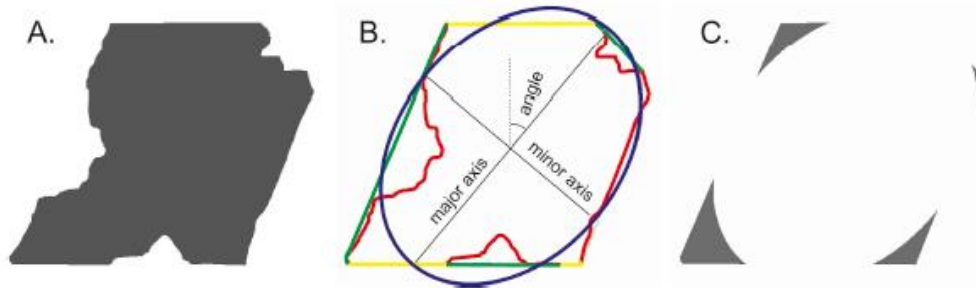
Figure 1. Principal of ore texture measurement. A: image of area object B: the red line is the perimeter of the object, the green line is convex-hull perimeter, and the yellow line is fitted ellipse. The yellow line is overlap green line with a red line. C: cookie cutter parameter, generated from object hull and ellipse (F. J.A. van Ruitenbeek et al., 2019)

Homogeneity and relative object size are two parameters that analyze homogeneous background in the mineral map and measure proportion image object with the background. Homogeneity compares convex hull from the largest object in the image with image area. Value 1 is the maximum value and has homogeneous background. Homogeneity can be calculated using equation:

$$\text{Homogeneity} = \frac{\text{convex hull area}_i}{\text{Image area}}$$

Relative object size compares the largest object area with image area. Value 1 means little cumulative object size to the background area, and reduction value from 1 indicate increase cumulative object (F. J.A. van Ruitenbeek et al., 2019).

$$\text{Relative object size} = \frac{\text{object area}_i}{\text{Image area}}$$
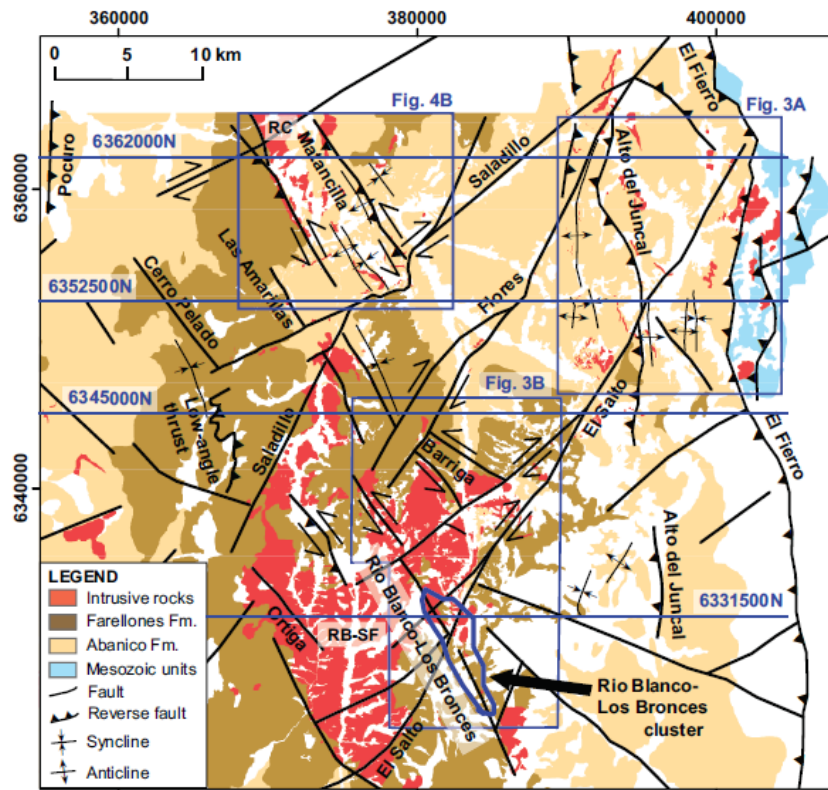
Figure 2. Geology of Los Bronces porphyry Cu deposit (Skarmeta et al., 2015)

2.3. Mineral spectroscopy

Spectroscopy is the study about the interaction between electromagnetic radiation of the energy and matter. The light energy as a function of wavelength can be emitted, reflected or absorbed by the material depend on the transition of the atom on the energy level. Reflectance spectroscopy is one of the spectroscopy method which applied energy in the visible (400-700 nm), near infrared (700-1000 nm) and short wave infrared (1000-2500 nm) wavelength region of the electromagnetic spectra to study the composition and structure of mineral (Hauff, 1983).

Short-wave infrared (SWIR) spectroscopy is widely used for mineral characterization as the typical spectra of minerals can be obtained in this region (Pontual et al., 1997a). The mineral composition can be recognized in the SWIR range due to the specific vibration of the interatomic bonding present on the crystal lattice of the mineral. The interatomic vibration is correlated to the absorbed energy at a particular wavelength. When a mineral is irradiated by the light, its atom can absorb the light at a certain wavelength. The infrared energy is not strong enough to generate electron excitation into a higher energy level as in UV energy. Infrared radiation can excite vibrations in molecular bonds.

The absorption band in the SWIR range is related to the stretching and bending vibration of the corresponding functional group. The SWIR spectra of each mineral depend on the composition, crystallinity, concentration and moisture content of the mineral (Hauff, 1983). The spectra analysis can be obtained by comparing the sample absorption spectra to the standard wavelength table which provide information on specific molecule vibration at a certain wavelength. Another method is by comparing the sample spectra with the spectra library on the instrument (Hauff, 1983). By identifying the molecule vibration corresponding to the spectra, the composition of the mineral can be obtained. The shifting of corresponding peak absorption wavelength can be used to identify the composition variation of mineral (Pontual et al., 1997).

Several absorption mineral groups that can be obtained from SWIR including clays, phyllosilicates, carbonates, micas, chlorites, sulfates, tourmaline, amphiboles, pyroxenes, garnets, pyroxinoids, silicates, evaporates, hydroxides, zeolites, and silica (). The general absorption molecules found in SWIR region that related to the mineral identification such as hydroxyl (OH), water (H_2O), carbonate (CO_2) and ammonia

(NH$_4$) (Pontual et al., 1997). Specific hydroxy absorption also found on the related vibration of AlOH, FeOH, and MgOH that also can be used to identify the mineral group component (Pontual et al., 1997).

Besides, the degree of crystallinity of minerals also can be acquired from the SWIR spectra. Crystallinity information can be generated by analyzing the shapes of the absorption peak. A sharp absorption peak implies the increase in mineral crystallinity (Pontual et al., 1997).

3. DATASETS AND METHODOLOGY

3.1. Dataset and material feasibility

A total of 43 hyperspectral images of milled pebbles samples were obtained from the previous research. The hyperspectral images were scanned by ITC Master student-Ms Agus, (2011) using SWIR the SisuCHEMA spectral imagery. The spectral SWIR camera produces high spatial resolution image with 0,2mm/pixels and 1000 - 2500 nm spectral range. This camera has 384 spatial pixels and 288 spectral bands. The complete specification can be seen on the table below (table 1). Several ancillary data were used in this study, as follows:

- XRF chemical analysis
  43 milled pebbles samples for Cu
- Thin section
  11 thin section obtained from TU Delft laboratory
- XRD analysis
  18 milled pebbles sample XRD qualitative analysis

All samples were obtained from Mr. Marinus Dalm-TU Delft.

In this research, several software will be performed, namely:

- ENVI (preprocessing image processing)
- Shaper script – IDL for extracting shape parameter of the image object (F. J.A. van Ruitenbeek et al., 2019)
- HyPpy (preprocessing and wavelength map (Bakker, 2012))

Table 1. SPECIM SISUchema spectral camera SWIR specification (SPECIM, 2015)

Optical Characteristic	Typical Specification
Spectral range	1000-2500 nm
Spectral resolution FWHM	12 nm (30 μm)
Spectral sampling	5.6 nm
Spectral resolution	rms spot radius <15 μm
F/#	F/2.0
Slith width	30 μm (50 or 80 μm optional)
Effective Slit length	9.2 mm
Electrical Characteristic	
Detector	Cyrogenically cooled MCT detector
Spatial pixels	384
Spectral bands	288
Pixel size	24 x 24 μm
Camera output	16 bits CL
SNR	1050:1 (at max signal level)

In this study, the methodology was divided into three main workflows. The first task was image pre-processing that focused on removing errors during image acquisition. The second step was image processing which includes wavelength mapping and decision tree classification which focused on mapping the mineral content on the hyperspectral images of the rock samples. The third step was the identification of ore texture geometry including basic shapes of grain, variation in shape and size, size, and object orientation using Shaper script. The result of the third step then analyzed using a statistical method to establish the relationship between texture geometry and copper grade. The detailed description of each step is given in the following sections.

3.2. RGB image visual Interpretation

The forty-three milled pebble samples were organized and classified into a group with the same characteristic. These groups were differentiated by visual differences. There were 4 classification parameters including rock texture, the color of rock matrix, color and size of the crystal.

3.3. Image pre-processing

The hyperspectral images were acquired using SicuCHEMA camera. The Digital Number (DN) was converted into reflectance using HypPy software package to identify the spectral characteristic of the minerals. After that, the image calibration was carried out using white and dark reference tool in HypPy software. Then, the spatial boundary of the rock sample images was manually digitized using region of interest (ROI) tool in ENVI. This ROI was used to mask out the background pixels of the images. The spectral subset in ENVI was applied to the input images to remove bands spectra that contain high noise level. The resulted spectral subset was 230 bands images covering the wavelength range between 1043 − 2486 nm.

The de-striping filter was applied to the input images using HypPy software to replace the bad pixel(s) that occurred due to miscalibration of the sensor camera. The de-striping filter was run twice, where the first run was focused on detecting the bad pixel and the second run to replace bad pixel using. In the first step, the maximum mean difference was set using value 10 and the maximum standard deviation of difference to 5. After that, the second step was applied, and the bad pixels were identified and then replaced. Lastly, the image spectral was smoothened though Mean 1+5+1 neighborhood filter in HypPy software package for the spectra with low noise level. Meanwhile, for the spectra with high noise level was smoothened using the Mean 5+9+5 neighborhood.

3.4. Image analysis

There were two steps that carried out in the image analysis. The first step was to do the wavelength mapping on the specific wavelength ranges in range 1850-2100nm and 2100-2400 nm for several mineral groups such as phyllosilicates, hydroxylated silicate, sulfates, carbonates and ammonium bearing minerals (Pontual et al., 1997). The result of the wavelength map was used to analyze mineral assemblage. A decision tree classification was performed to classify the mineral based on specified wavelength thresholds.

3.4.1. Wavelength map

The wavelength mapping is a technique to determines the location and depth of the absorption feature of mineral in a specific wavelength range of a hyperspectral image. The result of wavelength mapping is an RGB map containing information of the wavelength and depth of the deepest absorption feature of input images (Frank J.A. Van Ruitenbeek et al., 2014). The wavelength mapping technique able to map the mineral assemblage and distribution based on the position of the deepest absorption feature (Bakker, 2012). This absorption feature is directly related to molecular bond in their crystal lattice of mineral (Frank J.A. Van Ruitenbeek et al., 2014). The wavelength range of interest needs to be specified during the creation of the wavelength map.

The wavelength mapping required a specific input wavelength range as the target of mineral mapping. In this research, the wavelength range between 1850-2100nm and 2100-2400 were selected to targetting mineral groups such as AlOH, FeOH, and MgOH that have absorption feature within this region. The wavelength map was used to analyze mineral abundance on each sample images. Besides, it also used to locate the pure end members which show a deep absorption feature and good spectral signature.

3.4.2. Endmember

Mineral endmembers information was obtained from the previous researcher who analyzed milled pebble samples (Agus, 2011). Each of hyperspectral images of the rock samples was observed to find the what type of mineral type presence on the rock. The result then cross-checked and validated by using XRD data and thin section. The wavelength map also used for mineral type interpretation by analyzing scatter plot at

minimum absorption feature. After that, the ROI was used to define the endmember mineral spectra in the hyperspectral imagery rock sample. The average spectra were used as endmembers spectra. The obtained endmembers then used to construct a decision tree classification.

3.4.3. Decision tree classification

The decision tree classification is a tree-like classification model that uses a repetitive splitting of the input data into smaller component based on the tests of one or more criteria (Zhang et al., 2017). The criteria are built using if conditional of several parameters which determines whether the input data are split into the "Yes" or "No" branch. In this research, the decision tree model was built using the absorption feature characteristic of specific mineral that was observed in the wavelength map as the main parameters. Besides, the splitting parameter also includes the crystallinity index to differentiate some specific mineral that has similar absorption feature characteristic.

The absorption feature in the 2100-2400 nm range was set as the main parameter because it could separate mineral groups such as Al-OH, Fe-OH, MgOH and CO_3 group (Pontual et al., 1997). Moreover, the crystallinity index between water absorption at 1900 nm and Al-OH at 2200 nm was used to differentiate muscovite, high crystalline illite, and illite. The crystallinity index of Muscovite is 4. Meanwhile, high crystalline illite and illite has a crystallinity index of 3 (Pontual et al., 1997). In addition, the kaolinite index was also used to differentiate kaolinite and mixing based on the ratio of reflectance of wavelength 2160nm / 2180 nm. The classification results then were used to analyze the spatial distribution of mineral and ore texture using minimum wavelength absorption, depth of minimum absorption, white mica crystallinity and kaolinite ratio as input.
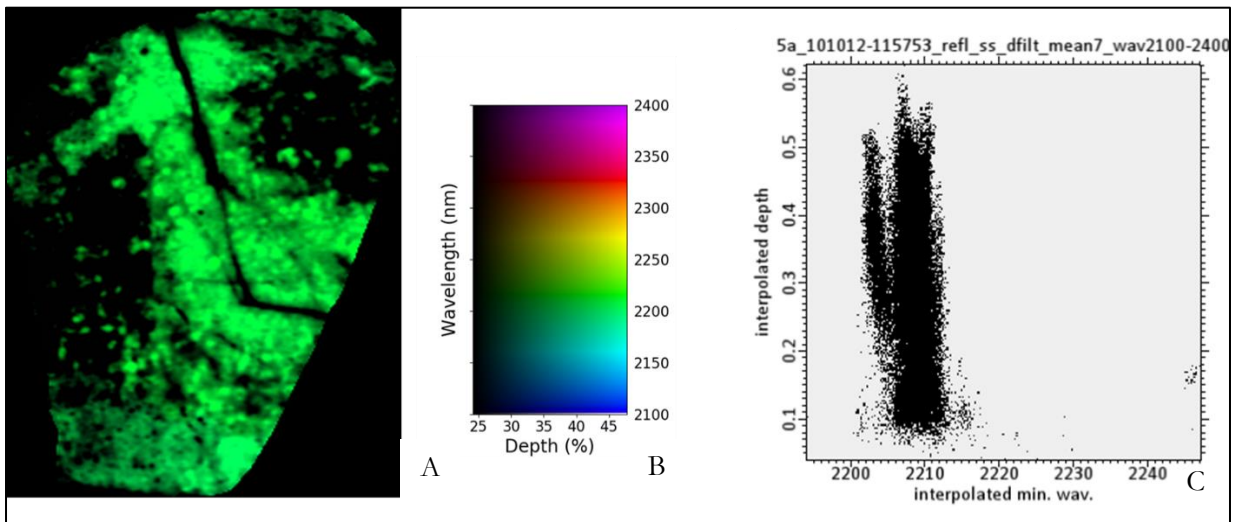

Figure 3. Example wavelength map from 2100-2400 nm wavelength range of sample 5a (A)RGB wavelength map (B) wavelength color scale (C) scatter plot of wavelength map.

3.4.4. White mica crystallinity

In the decision tree classification, white mica was differentiated by crystallinity ratio. White mica is a group of several minerals including muscovite, lepidolite phlogopite phengite, and illite. White mica, in general, has AlOH absorption feature at 2200 nm. The specific type of white mica was determined by calculating the ratio between the depth of AlOH absorption (wavelength domain of 1850 – 2100 nm and 2100 – 2400 nm) with the depth of water absorption at wavelength 1900 nm. According to Pontual et al. (1997b), by calculating this ratio, we can determine high crystalline illite that is characterized by shallow water absorption (around one-third of the depth of AlOH absorption. The white mica crystallinity can be calculated using equation:

$$\text{White mica crystallinity index} = \frac{\text{Depth Al-OH absorption}}{\text{Depth H}_2\text{O absorption}}$$

3.4.5. Kaolinite ratio

In the decision tree, kaolinite would be differentiated from illite kaolinite by using kaolinite ratio. Kaolinite clay spectra were characterized with doublet absorption around 2160 and 2200 nm, and 1400 nm associated with OH. Kaolinite crystallinity can be calculated using comparison depth of absorption feature at 2180 nm and 2160 nm. Band math in ENVI was used to calculate the ratio between 2160 and 2180 nm.

$$\text{Kaolinite ratio} = \frac{\text{Depth 2160 nm}}{\text{Depth 2180 nm}}$$

3.5. Validation of mineral classification

The mineral maps as the results of decision tree classification were validated using a confusion matrix. This matrix provided information about the accuracy of decision tree classification results. Here, random sampling was used for the validation process by choosing five samples. This technique was used to compare the classification results with the visual interpretation of the pixel's spectral signature. In the random sampling, some point was pinned in hyperspectral image randomly, then the pixel's spectra from each pinned-point were interpreted using spectral analyst tool in ENVI (with the USGS spectral library as a reference), XRD, thin section and visual interpretation. Both sampling results were compared with the mineral map derived from a decision tree classification and presented in a confusion matrix.

3.6. Ore texture measurement

The ore texture measurement was performed using shaper script with the mineral maps derived from the decision tree classification as input files. The algorithm extracted the edges of input images and calculated the geometric parameter of the shape which comes out in the results. The outcome of this algorithm is images and CSV file containing geometric parameters such as the total area, perimeter, compactness, roundness, convex, length, width, ratio, and angle of each mineral classes. Besides, it also extracts another geometric parameter such as the object center, object area, object perimeter, hull area, hull perimeter, ellipse area, ellipse perimeter, ellipse axes ratio, ellipse minor axis length, ellipse geographic orientation, object compactness, object roundness, object convexity, and cookie (F. J.A. van Ruitenbeek et al., 2019).

The shaper script was performed where the mineral maps as input were converted into the segmented images in the first step. The minimum object size was set to 200 pixels. The object shape parameter would calculate all object which had pixels more than 200. This set of pixels value has better accuracy than below 200 pixels for most object and shape parameter. Shaper software produces several images and csv file of shape parameter.

The ore texture measurement can be used to determine the various type of texture. The value in the rock texture measurement parameter was illustrated in the rock texture. In this research, several parameters were used to identify the texture such as flattening, relative object size, convexity, and standardize resultant. The function of each parameter on the ore texture determination is explained below.

Flattening is the ratio of the ellipse axis in shape parameter measurement. Flattening parameter determines the level of elongation of an object. The low flattening value reflects the vein shape. Meanwhile, the higher value corresponds to the spotted object. In this thesis, the threshold value to differentiate whether an object is a vein or spotted texture was 0.5 (F. J.A. van Ruitenbeek et al., 2019).

The convexity parameter applied to determine the crystal shape of the mineral class. The euhedral crystal is characterized by convex shape, well-formed crystal. On the other hand, the subhedral and anhedral crystal has less convexity and less-developed crystal. The threshold convexity values to differentiate these three crystal shapes are 1-0.95 for euhedral crystal, 0.95 - 0.7 for subhedral, and <0.7 for anhedral crystal (F. J.A. van Ruitenbeek et al., 2019).

Another shape parameter used in this research is relative object size. Relative object size was calculated from the largest object in the rock sample divided by the image area. This parameter compares the proportion of the largest crystal and clast in the image with a background image. The aphanitic has a value from 1 - 0.87, meanwhile the porphyritic texture has a range between 0.87 - 0.5.

Homogeneity is used to analyze homogeneous background in the mineral map with relative image proportion to the background. Homogeneity is the convex hull area of the largest object divides by image area of the rock sample. Value one determines aphanitic and porphyritic rock and 0.05 for phaneritic rock.

The orientation of crystal or clast was calculated by the angle between the vertical north of object with the major axis of the fitted ellipse. Standardize resultant parameter calculate the orientation of the object. The high value of standardize resultant reflect the oriented texture and the randomly oriented produce a low value of standardize resultant. The oriented value has value 1 and the randomly oriented texture has a value below 1.

4. RESULT

4.1. Visual interpretation of colour photo texture

Forty-three milled pebble samples with different texture were interpreted by visual analysis. The aim of the interpretation was to get the distribution type of texture. The main parameters in visual interpretation were:

- The texture of the pebble sample
- Color of matrix
- Color and size of crystal

Visual interpretation of 43 pebble sample resulted in five groups based on the parameters above. The first group characterized with an aphanitic texture which dominated with grey crystal, black crystal and white crystal with covered 9% from total pebble sample. This group recognized from fine grain crystal size and covered mostly with groundmass. Fine grain crystal indicates the rapid cooling of magma. Veinlet and spot of tourmaline appear in this group. Sample 133 show characteristic of this group (figure 4.1).

The second group was characterized with a brecciated texture which was dominated with black crystals as groundmass and grey crystals as phenocryst. Only one milled pebble sample has this characteristic. The clast of this breccia had angular-subangular shape and clast-supported with 25% matrix. The Donoso breccia has the same characteristic with this group. Sample 137 show characteristic of this group (figure 4.2).

The third group was described by porphyritic texture and dominated with grey crystal, white crystal, and black crystal. These were dominated almost pebble sample with 58%from total samples. 22 pebble had a similar characteristic, they were cut by veins. The proportion between groundmass and phenocryst around 20-40%. This texture has well-formed crystals and fine grain groundmass. This type of texture develops because of the different cooling process of minerals. Several milled pebbled in this third group have fractures and were filled with tourmaline mineral. Sample 2 shows the characteristic of the third group (figure 4.3).

The fourth group was indicated by porphyritic texture, dominated with red brownish crystal, pinkish crystal grey crystal, white crystal, and black crystal. This group could be recognized by red brownish-pinkish phenocryst. These groups covered 15% of the total pebble sample. The proportion of phenocryst and groundmass was around 20-40%. Some of the milled pebble cut by tourmaline and quartz veins. Sample 117 shows the characteristic of the fourth group (figure 4.4).

The last group was characterized by phaneritic texture and dominated with, red brownish crystal, grey crystal, and black crystal. Large size crystal is characteristic of this group and dominated with red-brownish phenocryst. This group covered 13% from 43 samples. Sample 4 show this characteristic (figure 4.5). The phaneritic texture of this group shows the large size of the crystal produced by the slow cooling and crystallization of magma. It indicates plutonic rock. This group can be interpreted as San Francisco batholith.

Table 2. 43 milled pebbles sample by visual interpretation classified to 5 group

| Group	1	2	3	4	5
Total samples in group	3	1	26	7	6
Classification properties					
Ground Mass	Grey crystal	Black crystals	Grey matrix	Red-brownish crystals	Red-brownish crystals
Crystals	white crystals	white crystals	Black crystals	Black crystals	Black crystals
	Black crystals	grey-green crystals	white crystals	White crystals	White crystals
	grey-green crystals			Red-brownish crystals	Grey crystal
				Pinkish crystals	
Textures	Aphanitic	Brecciated	porphyritic	porphyritic	phaneritic
Veins	black veins		black veins	black veins	Small black veins
matrix proportion	>95%	25%	20-40%	20-40%	<10%
Weathering	weak	weak	weak-medium	weak-medium	weak-medium
Characteristic	dominantly groundmass	Black crystals matrix	black vein	red-brownish matrix	euhedral-anhedral crystal
	fine-grain crystal	subangular-angular clast	Grey matrix	black vein	Black spot crystals
	black vein				
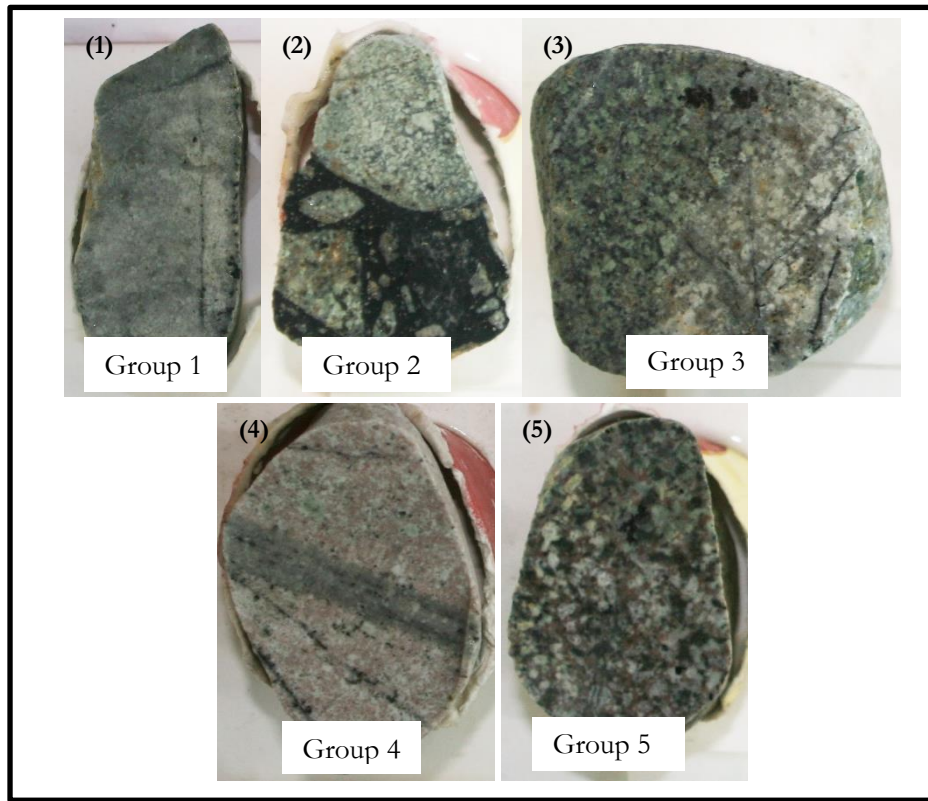
Figure 4. Milled pebble rock classification of group 1, group 2, group 3, group 4, and group 5

4.2. Endmember

Mineral endmember collection was extracted from milled pebble hyperspectral images in SWIR wavelength at 2.6 μm spatial resolution using the wavelength map and the ROI as a guide. The list of endmember spectra extracted is shown in table 3 and spectra presented in the figures 5-9 below.

Table 3. Diagnostic absorption feature spectra in endmember library

Mineral	1st absorption nm	2nd absorption nm	3rd absorption nm	4th absorption nm	comment
Illite short wavelength <2207nm	2190-2207	2337-2350	2430-2460		crystalinity lower than 3
Illite long wavelength >2207nm	2207-2220	2337-2350	2430-2460		crystalinity lower than 3
High crystalline illite short wavelength <2207nm	2190-2207	2337-2350	2430-2460		crystalinity lower than 4
High crystalline long wavelength >2207nm	2207-2220	2337-2350	2430-2460		crystalinity lower than 4
Muscovite short wavelength <2207nm	2190-2207	2337-2350	2430-2460		crystalinity higher than 4
Muscovite long wavelength >2207nm	2207-2220	2337-2350	2430-2460		crystalinity higher than 4
Tourmaline	2204-2215	2245-2260	2280-2305	2350-2365	
Chlorite	2245-2260	2320-2360			
Kaolinite	2200-2215	2160-2180			

4.2.1. White Mica

Illite and Muscovite are the most dominant mineral present in the all pebble milled sample. Muscovite and illite were determined by 3 diagnostic features (figure 5). The first absorption in the wavelength range from 2205-2211 nm due to vibrational absorption AlOH in the structure. Second and third absorption are found at 2337-2350 nm and 2430-2460 nm respectively.

In this research, white mica was divided into two group-based on the minimum wavelength position. According to the analysis of minimum wavelength position in the wavelength map, white mica has two

distributions. The short wavelength position of mica has spectra below 2207 nm, and the long wavelength is above 2207 nm. From this group, Illite can be further differentiated into a specific mineral based on crystallinity variation (Pontual et al., 1997). The crystallinity can be measured with the ratio of water absorption at 1900 nm and AlOH absorption at 2200 nm (Pontual et al., 1997). For example, the high crystalline illite has relatively shallow water absorption which is around one third or less of the AlOH absorption.
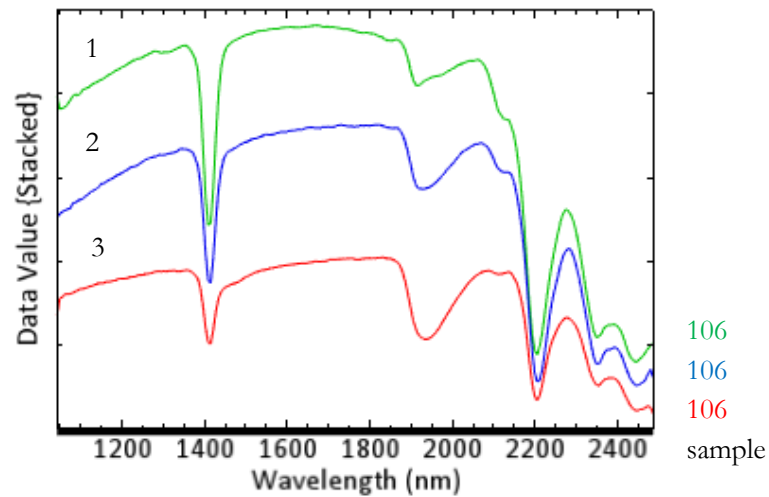
Figure 5. SWIR spectra of : 1; muscovite <2207nm (green line), 2; high crystalline illite <2207nm (blue line) and 3; illite(red line) <2207nm from sample 106
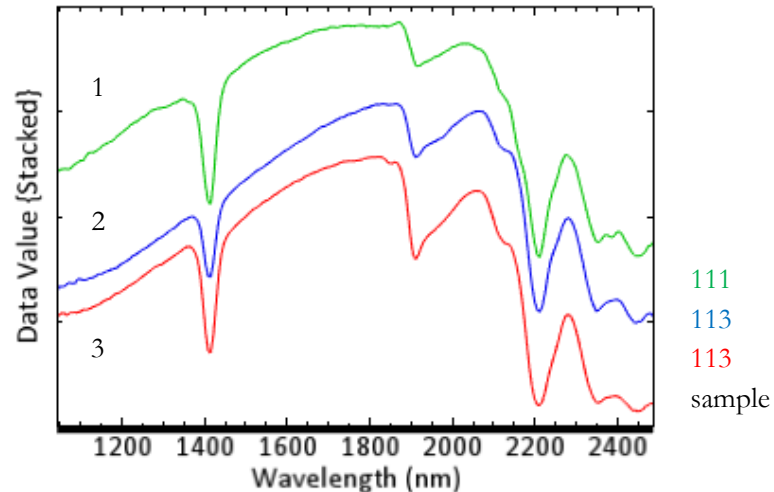
Figure 6. Spectra of: 1; muscovite >2207nm (green line), 2; high crystalline illite >2207nm (blue line) and 3; illite(red line) >2207nm from sample 113

4.2.2. Tourmaline

Tourmaline mineral can be determined by several absorption features at wavelength range 2100-2500 nm. The absorption feature can be recognized at 2204 nm, 2250 nm, 2300 nm, and 2365 nm as shown in figure 6. These absorption features represent the AlOH, MgOH, and FeOH vibration process (Clark et al., 1990). In short wavelength, tourmaline can be identified with a slight dip due to the effect of Fe^{2+} absorption (Pontual et al., 1997). Tourmaline minerals are an indicator of porphyry-style Cu-Au-Sn deposit (Baksheev et al., 2012).
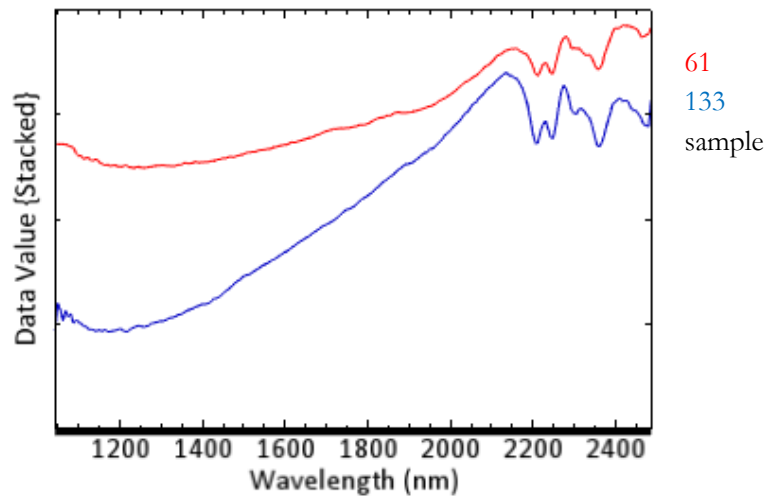
Figure 7. Spectra of tourmaline in hyperspectral images

4.2.3.   Kaolinite

Kaolinite minerals can be identified by diagnostic double absorption at 2160 nm and 2206 nm as shown in figure 8. The presence of kaolinite in the spectra is sometimes mixing with illite. The mixture kaolinite-illite can be measured by the ratio at 2160 nm and 2180 nm. Kaolinite can be recognized when the ratio value is more than one.
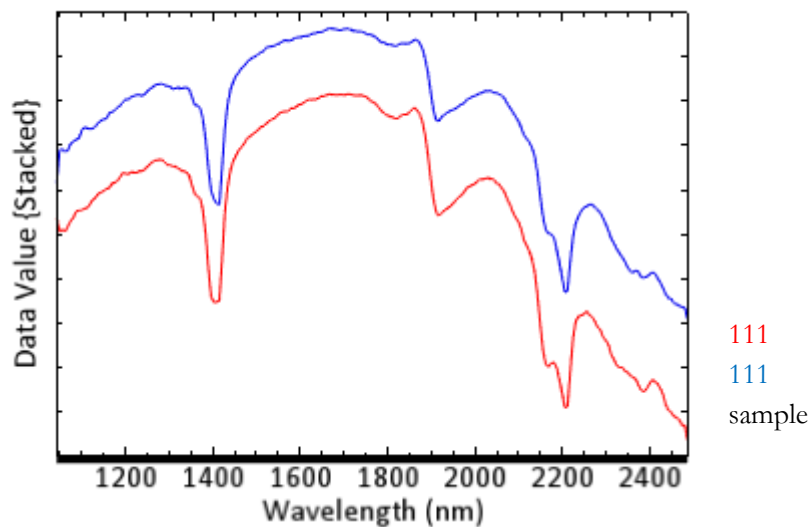

Figure 8. SWIR spectra of kaolinite (red line) and illite-kaolinite (blue line)

4.2.4.   Chlorite

Chlorite minerals can be identified by two main diagnostic absorptions between 2235-2255 nm and between 2320-2360 as shown in figure 9. The absorption around 2235 nm associated with FeOH and 2320 nm associated with MgOH (Pontual et al., 1997). When the absorption minimum shifts from shorter wavelengths to longer wavelengths, the chlorite composition slightly changes from Fe-rich to Mg-rich and vice versa.
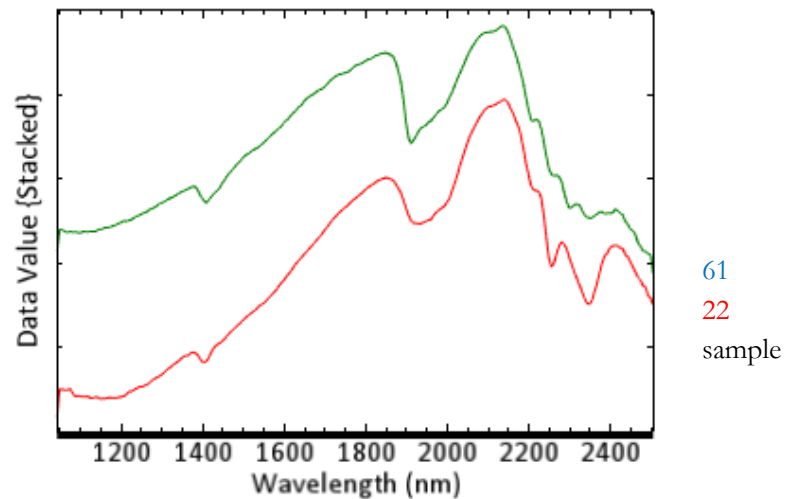
Figure 9. Spectra of chlorite from hyperspectral imagery

4.3.   Mineral classification map

The decision tree classification (figure 10) implements a multistage classification. This technique was applied to create mineral maps using wavelength map as the main parameter. The absorption feature at 2100-2400 nm range became the main branch due to a dominant absorption feature of Al-OH, Fe-OH, MgOH and CO_3 (Pontual et al., 1997). The ratio between water absorption at 1900 nm and Al-OH absorption at 2200 nm is used to differentiate the crystallinity index of muscovite, high crystalline illite and illite. Muscovite has high crystallinity with a ratio value of four; high crystalline illite has a ratio value of three while illite has ratio value lower than three (Pontual et al., 1997). The decision tree was used to discriminate minimum wavelength of white mica into long wavelength white mica and short wavelength white mica by determining wavelength threshold from lower than 2207 for short wavelength and greater than 2207 for long wavelength. Kaolinite index was used to differentiate kaolinite and mixing based on the comparison of the ratio at wavelength 2160nm/2180nm. The decision tree produces a mineral map and shows the spatial distribution of mineral. This result was used to analyze texture. The tourmaline class and chlorite class have an overlap on the absorption feature between 2320-2360 nm. The overlap between the Tourmaline and Chlorite class caused the decision tree classification to generate inaccurate mineral maps.

The mineral map generated from decision tree classification was validated by hyperspectral image, thin section, and XRD data. This validation used random point sample on hyperspectral images and then compared with the mineral map. Afterward, accuracy assessment was calculated using confusion matrices. This validation was used to analyze the accuracy and effectiveness of the decision tree classification. Confusion matrices were used to calculate the validation. Sample 4 has 80% overall accuracy and 0.56 of kappa score. Sample 6 has a 70% overall accuracy and 0.53 kappa score. Sample 62 has a 95% overall accuracy and 0.9 kappa score. The result of confusion matrices is presented in appendix 4.
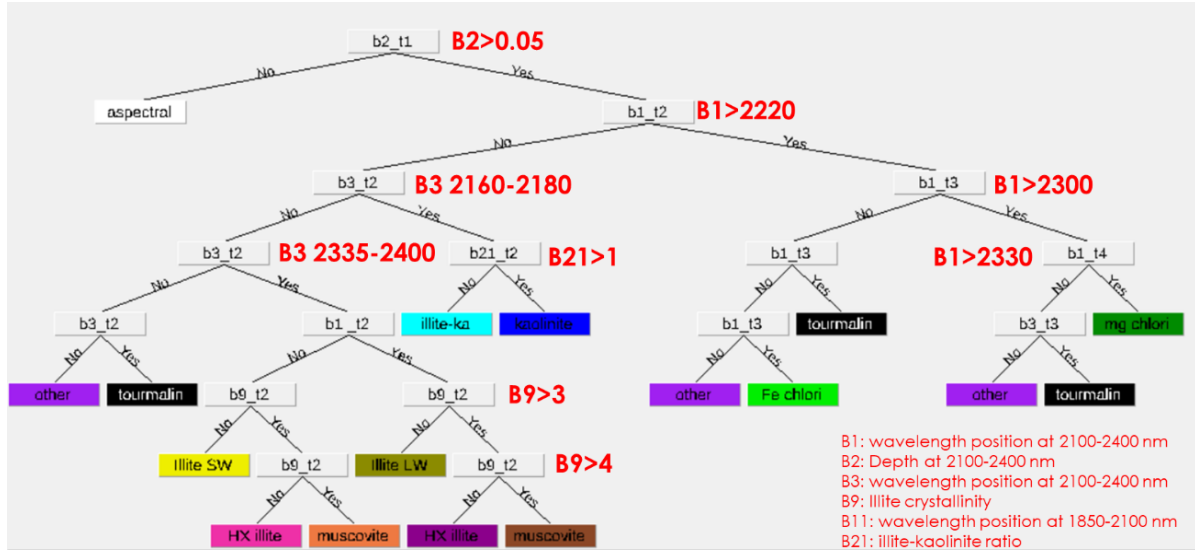
Figure 10. The decision tree classification generate mineral using wavelength map, illite, crystalinity

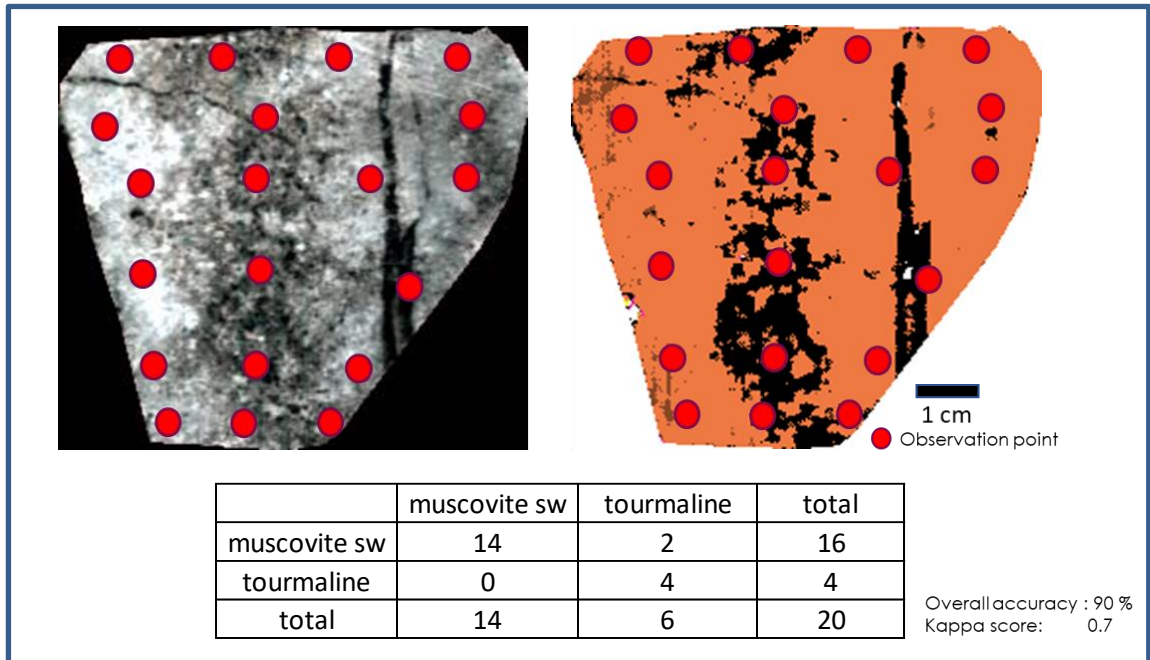|	muscovite sw	tourmaline	total
muscovite sw	14	2	16
tourmaline	0	4	4
total	14	6	20

Overall accuracy : 90 %
Kappa score: 0.7

Figure 11. Validation map using random point and confusion matrices at sample 132

4.4. Microstructure measurement

The result of visual interpretation, mineral map, and ore texture measurement was analyzed and compared to see the correlation between those three interpretations which associated with the ore texture. The sample was selected based on tourmaline bearing rock with the copper concentration from high to low. The reason for this analysis was to find out correlations rock texture measurement with copper enrichment. In addition, a different texture of tourmaline also analyzed.

The ore texture measurement can be used to determine the various type of texture. The value in the rock texture measurement parameter gives an illustration of the rock texture. In this research, several parameters such as flattening, relative object size, convexity, and standardize resultant were used to identify the rock

texture. The function of each parameter on the ore texture determination using 5 samples from the sample set is explained below. The rest of analyzed milled pebble sample are presented in appendix 1.

4.4.1. Sample 76 with 1.58% Cu

In the visual interpretation, sample 76 has grey color with grey groundmass, white crystal, black crystal as phenocryst and several crosscuts by veins (figure 12.1). In the mineral map, fracture filled with tourmaline and consist of short wave muscovite, short wave illite and short wave high crystalline illite as phenocryst. The pebble dominantly is composed of short wave muscovite which is formed by the alteration process XRD result of sample 76 shows that the pebble sample consists of quartz, muscovite, and pyrite. Based on the XRF analysis, sample 76 has the highest copper concentration with 1.58% of Cu.

Sample 76 has values one for homogeneity, which is calculated from the shape parameter. This value illustrates that the rock sample contains matrix. The relative object has value of 0.83, which indicates porphyritic texture and it reflects the proportion of crystal with the matrix.

The Pebble milled rock has fractures that are filled with tourmaline. Tourmaline A (see figure below) has flatenning value of 0.22. This shows the shape of the crystal is elongated. Crystal Tourmaline C has convexity value 0.53 that express the crystal has an anhedral form(table 4). The standardized resultant orientation of objects in the sample is 0.5, illustrating random orientation between vein and phenocryst. The mean orientation of the sample is pointing roughly to the north with 33 degrees (figure 12.4). The comparison of visual interpretation, mineral map, and texture measurement can describe the porphyritic texture and appearance of vein texture.
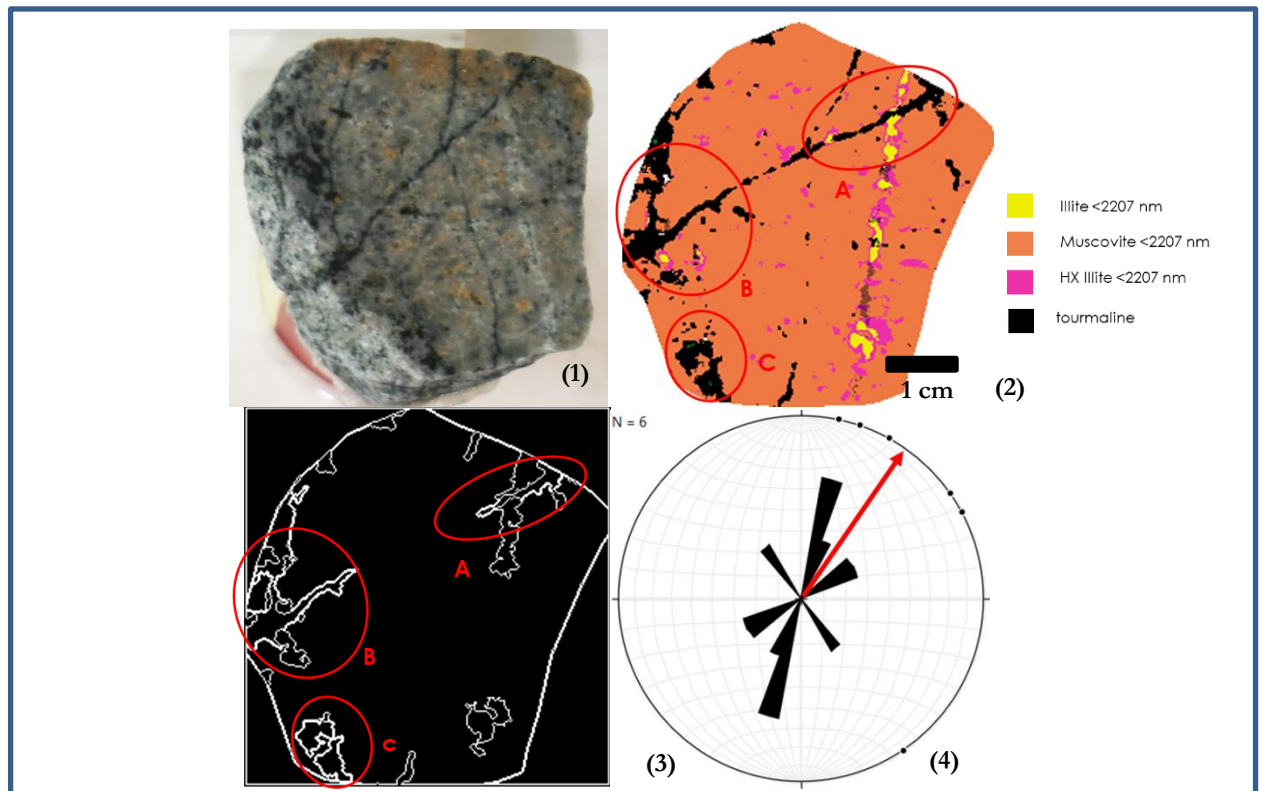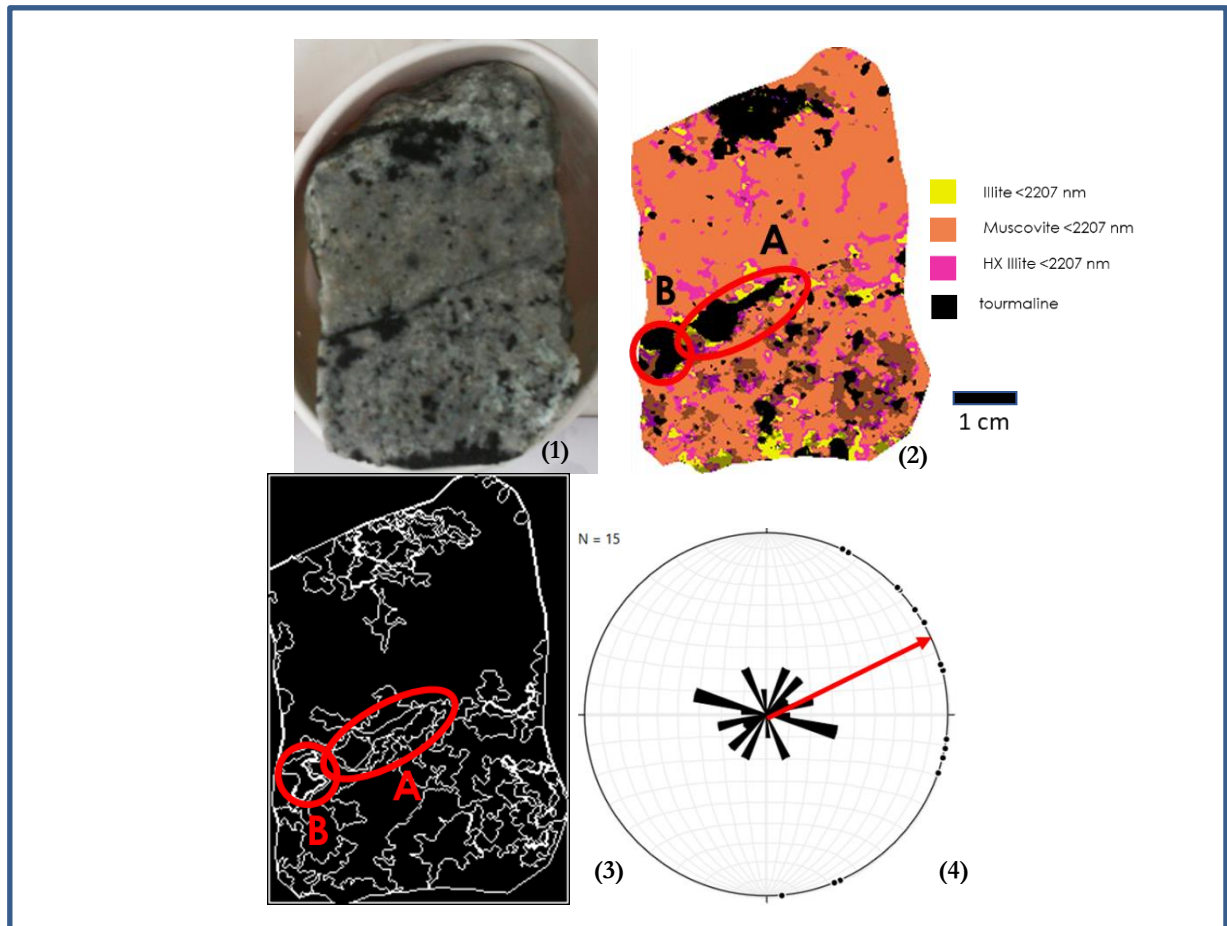

Figure 12. Color photo of sample 76 (1); mineral map classification from decision tree (2); object edge map from shaper (3) and rose diagram from mineral orientation.

Table 4. Microstructure measurement for sample 76a

sample	microstructure			orientation		banding
	number object	homogeneity	relative object	mean orientation	standardized resultant	
76a	7	1.0	0.83	33	0.53	0
	Object size (pixels)	mm	Flattening	Cookie cutter	Convexity	Compactness	Hollowness
tourmaline A	409	81.8	0.22	0.13	0.82	0.18	0.53
tourmaline B	675	135	0.47	0.06	0.61	0.21	0.71
tourmaline C	1644	328.8	0.48	0.19	0.53	0.07	0.34

4.4.2. Sample 10 with 1.52% Cu

Sample 10 is a porphyritic sample which has grey color with veinlet and black crystals based on visual interpretation(figure 13.1). The mineral class map shows muscovite short wave as groundmass which was produced during the alteration process. Besides that, high crystalline illite shortwave, high crystalline illite long wave, illite short wave, illite long wave, and tourmaline also present on the sample. XRD result show some mineral quartz, muscovite, chalcopyrite, and pyrite. The mineral map also indicates the vein texture and disseminated tourmaline, which is the same as in the visual interpretation. Based on the XRF analysis, sample 10 has copper concentration with 1.58%.

Sample 10 has values 0.95 for homogeneity which illustrates the presence of a matrix. The relative object has value of 0.55 which indicate porphyritic texture, and it reflects the proportion of phenocryst within the matrix. The milled pebble rock fractured with tourmaline infilling. The crystal tourmaline A, show the flattening value 0.33 (see figure below). It shows the crystal has a vein shape. Crystal Tourmaline B has convexity value 0.81 which expresses that the crystal has a subhedral form (table 5). The standardized resultant of the sample is 0.26, illustrating random orientation. The vein and phenocryst have a different direction and illustrate random orientation. Ore texture measurement can depict the vein and porphyritic texture which gave a similar result to mineral map and rock image.
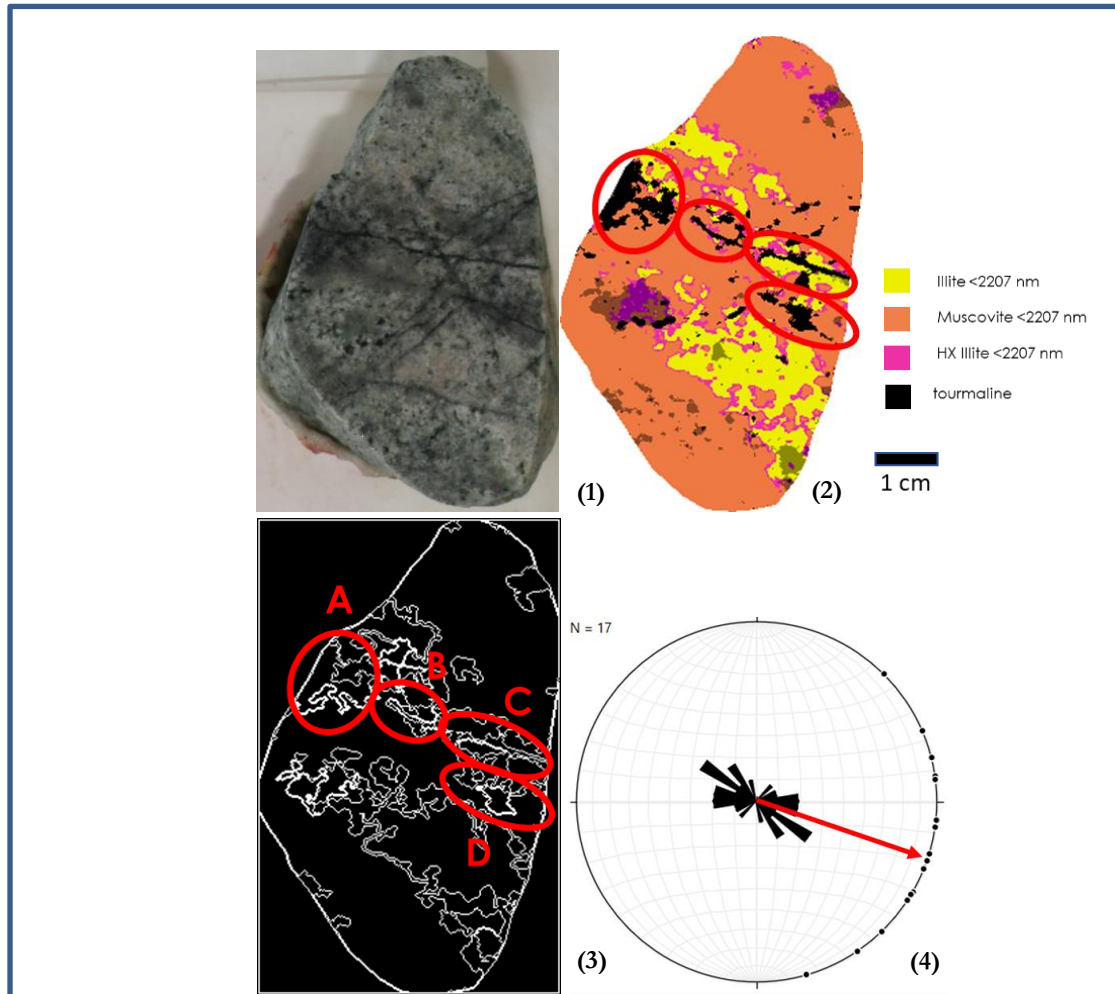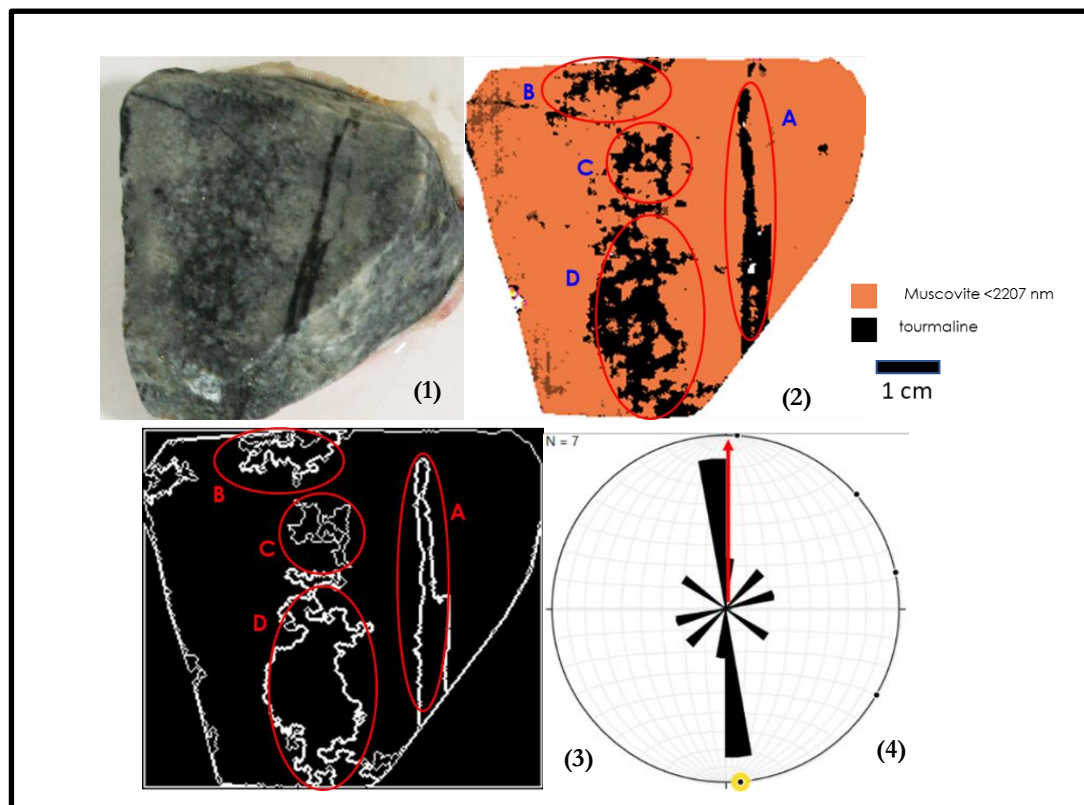
Figure 13. Color photo of sample 10 (1); mineral map classification from decision tree (2); object edge map from shaper (3) and rose diagram from mineral orientation.

Table 5. Microstructure measurement for sample 10a

sample	microstructure			orientation		banding
	number object	homogeneity	relative object	mean orientation	standardized resultant	
10	16	1.0	0.55	66	0.26	0
	Object size (pixels)	mm	Flattening	Cookie cutter	Convexity	Compactness	Hollowness
tourmaline A	927	185.4	0.33	0.11	0.83	0.29	0.68
tourmaline B	732	146.4	0.82	0.09	0.81	0.44	0.78

4.4.3.   Sample 62 with 0.95% Cu

Visually, sample 62 has grey color with grey groundmass, white crystal, black crystal as phenocryst and stockwork texture (figure 14.1). In the mineral classification map, fracture filled with tourmaline and consist of short wave muscovite, short wave illite and short wave high crystalline illite. The pebble is dominantly composed by short wave muscovite which is formed by alteration process. XRD result shows that the pebble consists of quartz, muscovite and pyrite. Based on the XRF analysis, sample 62 has 0.95% of Cu.

Sample 62 has value one of homogeneity which illustrates the presence of a matrix. The relative object has score of 0.6, which indicate porphyritic and it reflects the proportion between phenocryst and matrix.

Pebble milled rock has stockwork texture filled with tourmaline mineral. Tourmaline B and C has a flattening value of 0.34 and 0.14 respectively which indicate elongation shape and stockwork texture(table 6). Crystal

Tourmaline A has value 0.84 at convexity; it expresses the crystal has subhedral form. The standardized resultant of the sample is 0.5, illustrating random orientation between stockwork and phenocryst. This was similar to the result of the mineral map and rock image. Ore texture measurement can depict information of stockwork, porphyritic and random orientation of the rock sample.
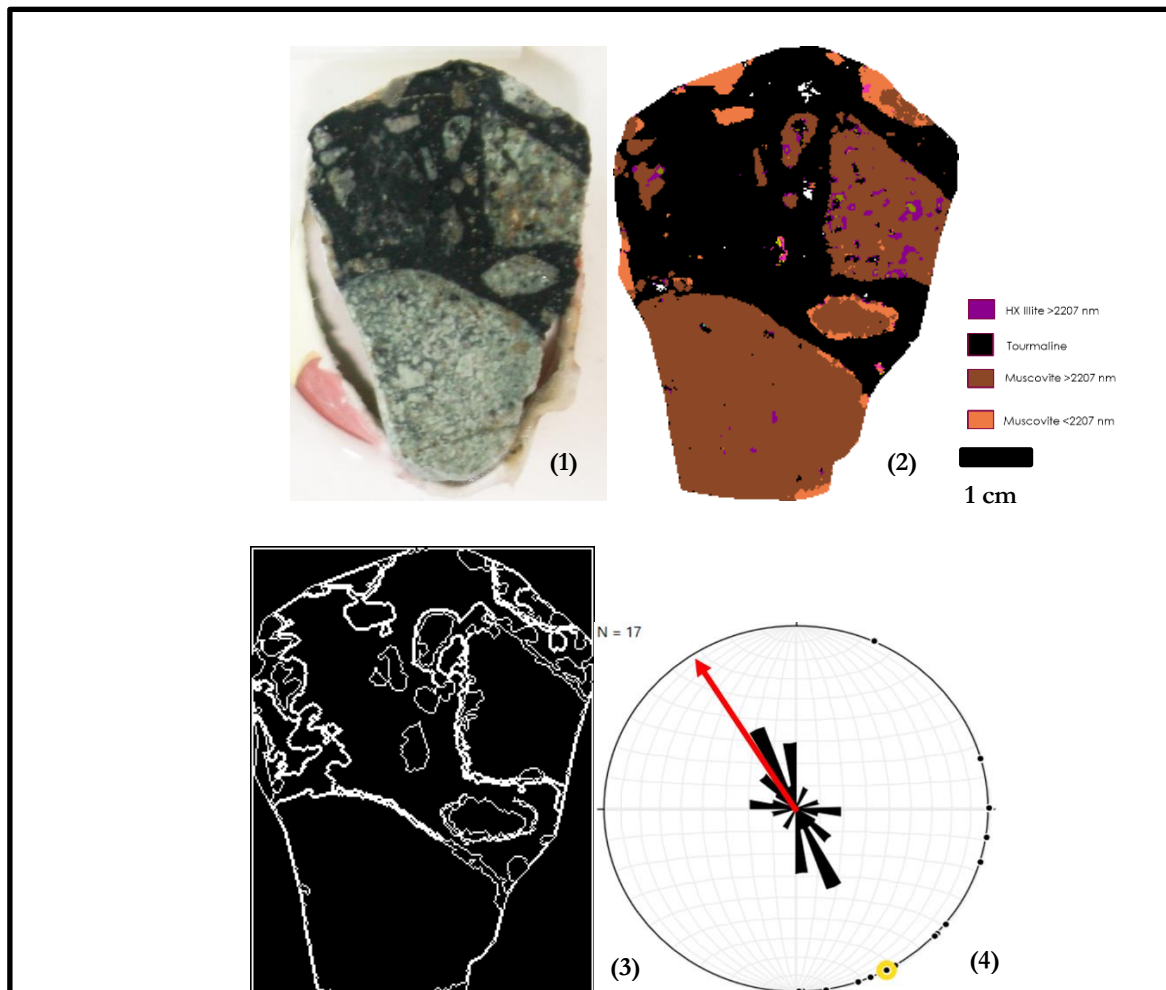

Figure 14. Color photo of sample 62 (1); mineral map classification from decision tree (2); object edge map from shaper (3) and rose diagram from mineral orientation.

Table 6. Microstructure measurement for sample 62

sample	microstructure			orientation		banding
	number object	homogeneity	relative object	mean orientation	standardized resultant	
62	18	1.0	0.60	108	0.5	0
	Object size (pixels)	mm	Flattening	Cookie cutter	Convexity	Compactness	Hollowness
tourmaline A	304	60.8	0.61	0.09	0.84	0.41	0.78
tourmaline B	316	63.2	0.14	0.15	0.81	0.12	0.47
tourmaline C	226	45.2	0.34	0.01	0.70	0.11	0.38
tourmaline C	1241	248.2	0.79	0.09	0.49	0.11	0.60

4.4.4. Sample 132 with 0.49% Cu

Based on the visual interpretation, sample 132 has grey color with grey groundmass, white crystal, black crystal as phenocryst and vein texture (figure 15.1). In the mineral classification map, fracture fills with tourmaline and consist of short wave muscovite; The pebble dominantly was composed by short wave muscovite which is formed by the alteration process.

Sample 132 has the value of one for homogeneity. The relative object size has score 0.78 (table 7), which indicate porphyritic texture.

Tourmaline A has 0.11 of flattening value that reflects vein structure. The standardized resultant of the sample is 0.3, illustrating random orientation between the vein and disseminated tourmaline mineral. Comparison between ore texture measurement, rock photo, and mineral map, give a similar finding that the rock sample has a vein structure.

Figure 15. Color photo of sample 132 (1); mineral map classification from decision tree (2); object edge map from shaper (3) and rose diagram from mineral orientation.

Table 7. Microstructure measurement for sample 132

sample	microstructure			orientation		banding
	number object	homogeneity	relative object	mean orientation	standardized resultant	
132	8	1.0	0.78	1	0.3	0

	Object size (pixels)	mm	Flattening	Cookie cutter	Convexity	Compactness	Hollowness
tourmaline A	1534	306.8	0.11	0.10	0.86	0.14	0.64
tourmaline B	678	135.6	0.35	0.12	0.56	0.13	0.59
tourmaline C	645	129	0.74	0.07	0.52	0.12	0.56
tourmaline D	3759	751.8	0.42	0.19	0.43	0.08	0.53

4.4.5. Sample 137 with 0.23% Cu

Visually, sample 137 has grey color with black groundmass, white crystal, black crystal as clast. In the mineral classification map, tourmaline present as matrix and long wave muscovite as clast (figure 16.1). XRD result shows the presence of breccia consists of quartz, muscovite, pyrite, and orthoferrosilite. The value 0.7 of homogeneity parameter illustrates brecciated texture and the value 0.32 of relative object size parameter show the corresponding proportion of objects, between clasts and matrix. Based on the XRF analysis, sample 137 has 0.23% of Cu.

The clast of short wave and long wave muscovite have an average flattening value of 0.5 (table 8). It shows the angular shape of the clast. The standard resultant of brecciated pebble sample has value 0.5 which indicates a random orientation of clast breccia texture. The tourmaline hollowness has value 0.62 which indicate that the rock sample has hollow surface and can be described as brecciated texture. This rock measurement corresponds to the rock photo and mineral map which also shows brecciated texture.

Figure 16. Color photo of sample 137 (1); mineral map classification from decision tree (2); object edge map from shaper (3) and rose diagram from mineral orientation.

Table 8. Microstructure measurement for sample 137a

sample	microstructure			orientation		banding
	number object	homogeneity	relative object	mean orientation	standardized resultant	
137	17	0.7	0.32	327	0.5	0

	Object size (pixels)	mm	Flattening	Cookie cutter	Convexity	Compactness	Hollowness
tourmaline A	18178	3635.6	0.90	0.12	0.61	0.21	0.62

4.5. Data integration

4.5.1. Copper grade of Tourmaline bearing rock and Non-Tourmaline bearing rock

Tourmaline is formed through the hydrothermal process which occurs at the same time with copper mineralization (Skewes et al.,2003). Therefore, tourmaline is regarded as a characteristic of the existence of copper in porphyry deposit (Baksheev et al., 2012). The comparison of rock containing tourmaline and non-tourmaline versus copper content was constructed to investigate the correlation between tourmaline and copper content. About 18 rock samples containing tourmaline and 25 rock samples without tourmaline was used to create the sample graph as a function of copper content.

A scatter plot of milled pebbles containing tourmaline mineral and non-tourmaline mineral is shown in figure 17. Black dashed line indicate the cut-off grade of 0,4%. Cut-off grade 0.4% is the minimal copper concentration to be economically mined. Based on the samples distribution, 11 of the milled pebbles have a high content of copper, and seven milled pebble samples have copper content below the cut-off grade. In figure 17.b, there are eight milled pebbles from the total sample which has an economical value of copper, while 17 samples have a low content of copper. The average copper content of tourmaline bearing rock is 0.69% and non-tourmaline rock bearing mineral has 0.38% of copper content. It can be seen that tourmaline bearing rock has a higher average of copper content than non-tourmaline bearing rock. An anomalous result appears in the non-tourmaline graph, where sample 107 has a high content of copper compared to other samples. This abnormality result may have occurred probably because of error during XRF measurement.
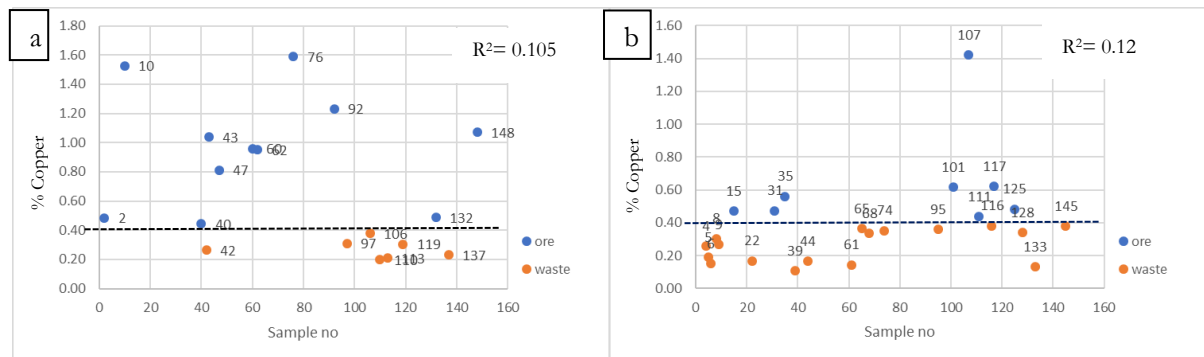
Figure 17. Scatter plot of milled pebble contain tourmaline mineral (a) and non tourmaline (b) as a function of copper grade

4.5.2. Tourmaline parameters and Copper grade

As mentioned above, tourmaline bearing rock had a high concentration of copper content. Therefore, tourmaline can be used as an indicator of high copper content within the samples. This finding was used as a mineral selection parameter. Only tourmaline mineral was used for texture analysis. About 18 rock samples contain tourmaline mineral was observed to extract the texture measurement and then analyzed to find the relationship with the copper content.

4.5.2.1. Convexity

Figure 18 illustrates the convexity values distribution of the tourmaline mineral. Based on the graph, convexity was divided into three classifications, euhedral, subhedral and anhedral. It can be seen that both tourmalines are categorized as ore and waste group in the milled pebble sample generally has subhedral and anhedral crystal shape. This tourmaline crystal shape is related to the hydrothermal process. The rapid cooling makes subhedral-anhedral crystal form. In visual interpretation and mineral map, tourmaline mineral appears as vein and individual crystal.

The regression lines can be used to determine the correlation between variables in the graph. The obtained regression value is 0.03 which indicate a low correlation between convexity and copper grade. Hence, it can be deduced that Cu grade is almost independent with the convexity parameter of rock texture.
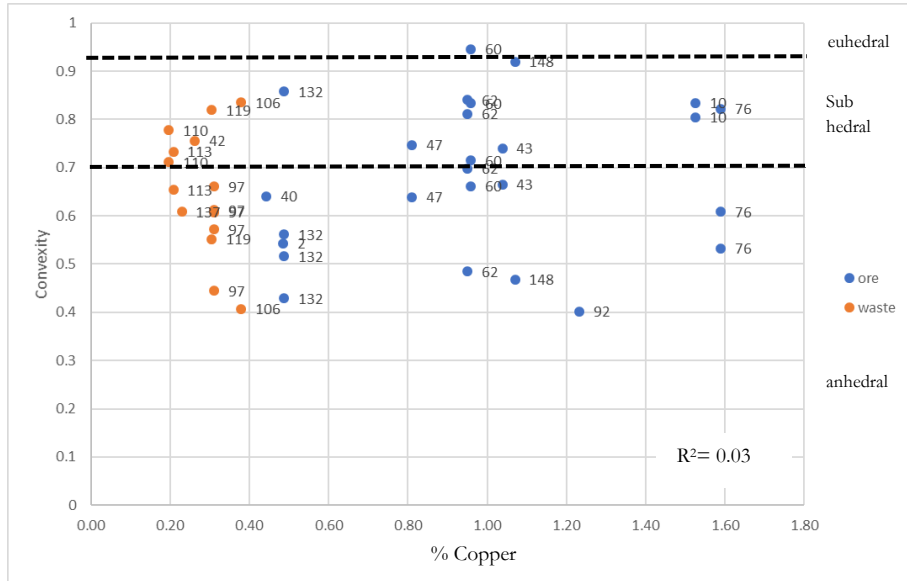
Figure 18. Scatter plot of tourmaline convexity versus copper grade, tourmaline mineral dominantly appears in subhedral-anhedral shape.

4.5.2.2. Flattening

The scatter plot of flattening value versus copper grade is shown in Figure 19. Based on the graph, five samples with a high concentration of copper have low flattening value which indicates the tourmaline has an elongated shape. Based on the visual interpretation, sample 76, 10, 92, 62 and 60 has a vein texture and fill with tourmaline mineral. It can be seen that the high concentration of copper is related to the low flattening value or elongated shape, which represent vein shape.
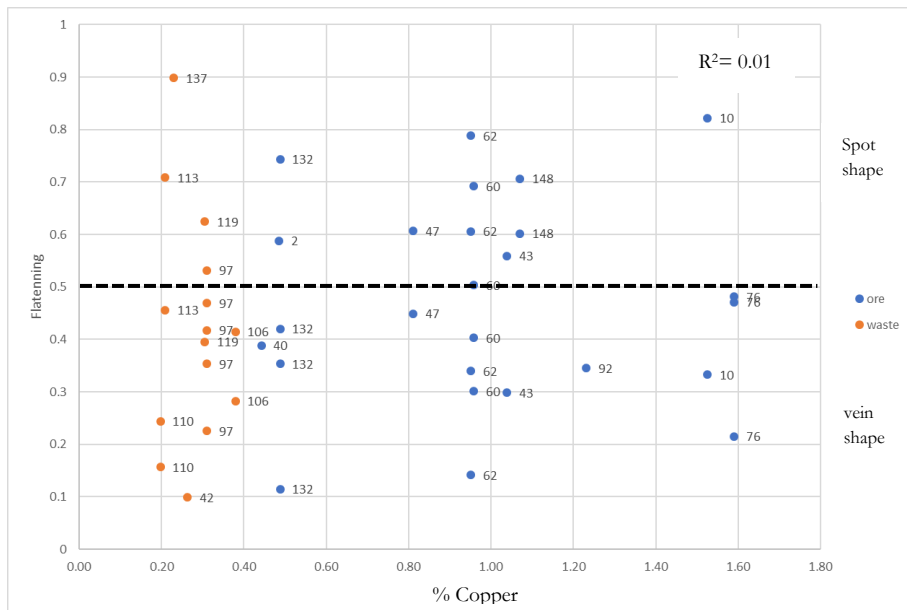
Figure 19. Scatter plot of flattening versus copper grade. Tourmaline mineral contain high copper concentration has low value of flattening. Low flattening reflects elongated shape. It is related to vein structure.

4.5.2.3. Relative object size

Figure 20 illustrates the relative object size of the milled pebbles sample. According to figure 20, the milled pebble sample with the copper content above the cut-off grade generally has porphyritic texture, while a low copper content sample had various type of texture. The porphyritic texture related to Donoso breccia clast, monzonite rock with porphyritic texture. The texture classification using relative object size was calculated from ore texture measurement shown good accuracy compared to the visual interpretation. According to R^2 value, relative object size and Cu grade have low correlation. However, samples with porphyritic texture and tourmaline bearing show increase in Cu concentration with increasing relative object size
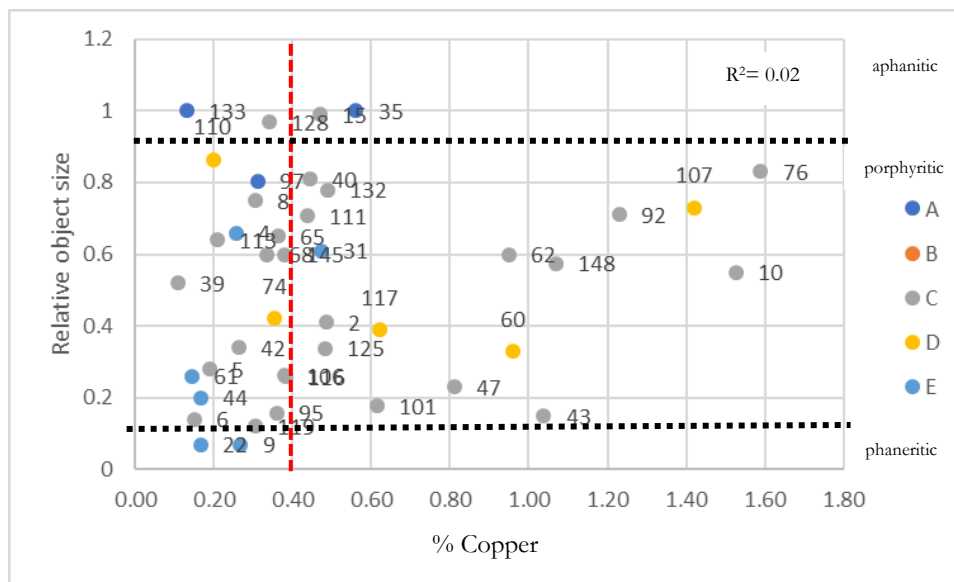
Figure 20. Scatter plot of relative object size versus copper grade, blue dot A as group 1 in visual interpretation, B as group 2, C as group 3, D as group 4 and E as group 5.

4.5.2.4. Orientation

Figure 5 shows the standardize resultant parameter value of the milled pebbles versus copper grade. Based on the distribution of standardize resultant value, both milled pebbled above and below cut-off grade has the same random orientation. However, none of the oriented clast samples has high copper content. The milled pebble samples code 76, 10, 92, 148 and 43 have high copper content, porphyritic texture, and vein texture. The phenocryst and vein contribute to a different direction or random orientation of the rock sample.
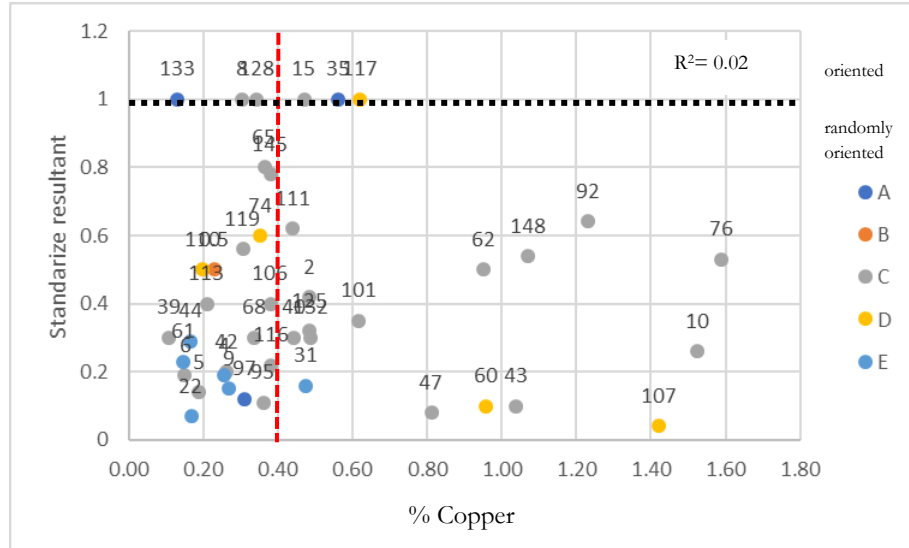
Figure 21. Scatter plot of standarized resultant with a copper grade, blue dot A as group 1 in visual interpretation, B as group 2, C as group 3, D as group 4 and E as group 5

5. DISCUSSION

Visual interpretation has been conducted for 43 milled pebble samples. The analysis generated five groups of milled pebble samples which based on the parameters such as texture, color, and size.

The first group was indicated by the presence of aphanitic texture. The veinlet and aggregate of tourmaline appear in this group. Figure 4.1 show, grey fine grain crystal covered the rock and crosscut with tourmaline vein halo. Fine grain crystal indicates rapid cooling crystallization. This group can be generated from post mineral rock of Los Bronces porphyry. Which are characterized by Dacite and Latite rock with aphanitic texture.

The second group was characterized by brecciated texture. Figure 4.2 show sample 137 with brecciated texture, angular-subangular grey clast and black groundmass. The sample in this group have similar characteristic with The Donoso breccia which Skewes et al.,2003 described in their research., where the tourmaline is groundmass.

The third group was characterized by porphyritic texture Figure 4.3 show, milled pebble samples with porphyritic texture, having grey mineral as groundmass and black crystal, white crystal as phenocryst. Black crystal appears as veinlet and disseminated texture. This group has a similar characteristic tourmaline breccia clast. It is described as quartz monzonite with stockwork and disseminated texture.

The fourth group was represented with a porphyritic. Figure 4.4 sample show, milled pebbles with porphyritic texture and cross cut by grey crystal. This group has similarities with the clast of Donoso breccia which is described d as a monzonite (Skewes et al., 2003).

The last group was characterized by phaneritic texture Figure 4.5 from sample xx, show milled pebble with phaneritic texture, and disseminated black crystal. This group can be interpreted as San Francisco batholith. San Francisco batholith composed of quartz monzonite and quartz monzodiorite with fine to coarse grain and porphyritic to equigranular.

Tourmaline bearing rock and non-tourmaline bearing rock (figure 17) shows that high content of copper is correlated with the rock containing tourmaline. Most of the rock sample containing tourmaline stand above the cut-off grade. It can be deduced that tourmaline mineral can become an indicator of the presence of copper content. According to Skewes et al., 2003, mineralization on Los Bronces is associated with tourmaline-bearing Donoso breccia. The Donoso breccia, characterized by monolithic clast with quartz monzonite. Its breccia matrix is containing tourmaline, quartz, pyrite, chalcopyrite, specularite, and lesser amounts of anhydrite and bornite.

The ore texture measurement can be used to determine the various type of texture. In this research, several measurements were used to identify the texture such as flattening, relative object size, convexity, and standardize resultant. The function of each parameter on the ore texture determination is explained below.
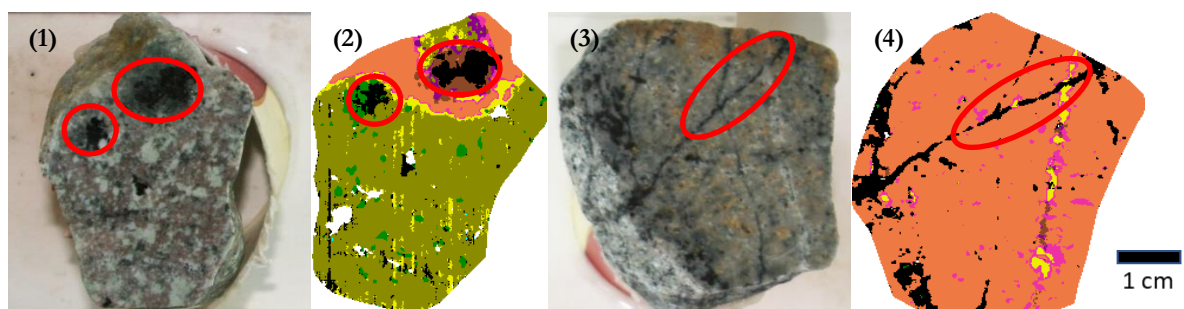
Figure 22. Color photo and mineral map of milled pebbles with spot/disseminated structure at (1&2) sample 113 with 0.21% Cu and (3&4) veinlet structure at sample 76 with 1.59% Cu

• Flattening

As mentioned above, tourmaline mineral was selected to analyses the shape parameter including flattening and convexity. Flattening can be distinguished the spot and vein shape. The tourmaline mineral has an elongated shape that implies to the vein shape when the flattening value less than 0.5. The tourmaline has spotted shape when the flattening value is bigger than 0.5.

RGB image and the mineral map shows that sample 113 has spot/individual mineral. In the rock texture measurement, tourmaline mineral A has flattening value of 0.7 and b 0.5 which illustrate as individual/spot mineral. This sample contains 0.21% Cu based on the XRF measurement.

RGB image and mineral map shows that sample 76 has vein structure. This texture has 0.2 flattening which indicates an elongated shape or vein shape. This sample has 1.59% Cu.

Vein texture is related to the fracturing of the rock during the hydrothermal process. During this process, the hydrothermal fluid which contains copper bearing will mineralize on the rock. Stockwork and disseminated texture also formed during this process. Based on figure 18, the low value of flattening represents a high concentration of copper. It is confirmed that low value flattening correlated with vein texture, which brings mineralization of copper on the rock sample. In addition, as the stockwork and disseminated texture formed during the same process with hydrothermal process, these textures also can be used to identify the presence of high copper content on the rock sample.
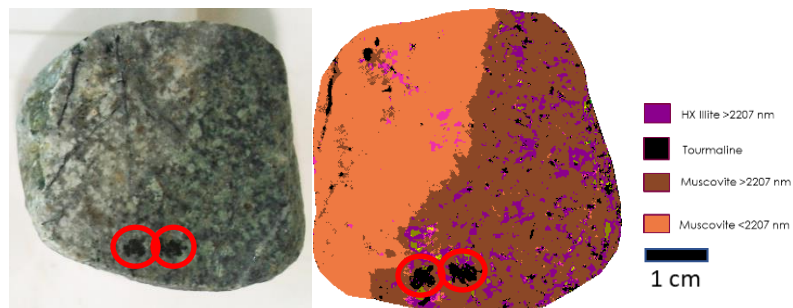
Figure 23. Tourmaline mineral with subhedral-anhedral crystal shape.

• Convexity

Convexity parameter can be applied to assign the shape of phenocryst in igneous rock or angularity for sedimentary rock. In igneous rock, the shape of the parameter has an important role to determine the degree of crystallization. A well-developed crystal or euhedral is formed by the slow cooling process, and anhedral crystal is formed via rapid cooling. Figure 19 shows the tourmaline mineral with a high concentration of copper from Los Bronces, present in the euhedral-subhedral form. This is related to tourmaline mineral which appears during the hydrothermal process with rapid cooling has a euhedral-subhedral shape (Skewes et al., 2003).

Figure 23 shows the milled pebble sample 2 which has tourmaline mineral with convexity value 0.5 and 0.7 which indicates anhedral crystal shape. The comparison between the visual image, mineral map and rock texture give a similar result that shape of tourmaline mineral is anhedral. This process is due to infill in the hydrothermal process (Taylor, 2009).

• Relative object size

The relative object size measures the proportion between crystal or mineral with object background or matrix. This proportion is correlated with the mineral distribution or rock texture on the igneous rock. A high value of relative object size indicates aphanitic texture, while a low value of relative object size represents porphyritic

and phaneritic texture. Figure 20 shows the comparison of relative object size classification result with the visual interpretation. The classification of relative object size and visual interpretation has a similar result which dominantly by porphyritic texture. The mineral map also shows a similar result as a visual interpretation. The low accuracy of the mineral map can be caused by the process of the decision tree classification. The interpretation generated from the decision tree may become inaccurate due to wrong input expression for the mineral classification or overfitted classification on the decision tree. An example for this case can be seen in sample 6 which has 70% mineral map accuracy as the chlorite and tourmaline have misclassified due to the same location of the first deepest absorption at 2350. Another reason is because of the limitation of the hyperspectral image. The SWIR range only able to detect several groups of minerals, thus undetected minerals may cause wrong interpretation of the hyperspectral image and created an incorrect mineral map. As a consequence of the incorrect mineral map, the mineral map generates different interpretation from the visual observation and different rock texture.

Based on figure 24, the relative object size parameter and copper content did not relate. Thus, the relative object size cannot be associated with copper content. However, at high concentration of copper with the value above cut-off grade, the rock sample has porphyritic texture and contain tourmaline. According to Skewes et al., 2003, high copper content exists in the Donoso breccia formation which has quartz monzonite clast with porphyritic texture.
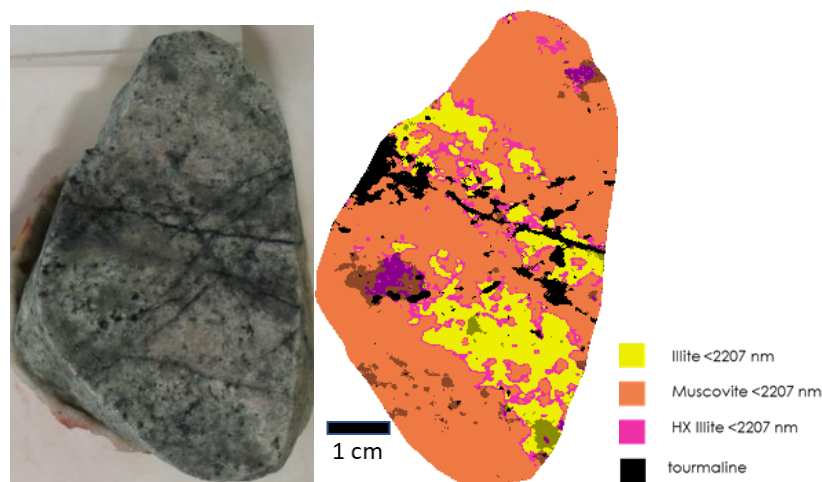
Figure 24. Sample 62 has 0.5 value of standardize resultant**,** it indicates random orientation. vein and phenocryst orientation have different direction.

• Standardize resultant

The standardize resultant was used to determine the orientation of phenocryst or vein on the rock sample. The high value of standardize resultant correlated with the oriented direction while low value means random orientation. For example, in the figure 24 show sample 62 has standardize value 0.5 which reflects random orientation of the crystal. It can be seen in the sample 62 which has vein with the relative northwest-southeast direction and the phenocryst has random direction. It will produce a low value of standardize direction which indicate random direction.

According to the graph in figure 21, the high concentration of copper has random direction, but none of preferred orientation has high content of copper. This can be seen in the milled pebbled which has random orientation because the vein structure and phenocryst on the porphyritic texture don't have the same direction. The phenocryst on the porphyritic texture is formed in crystallization of magma with various orientation of the crystal. The direction of vein texture depends on fracture in the hydrothermal process.
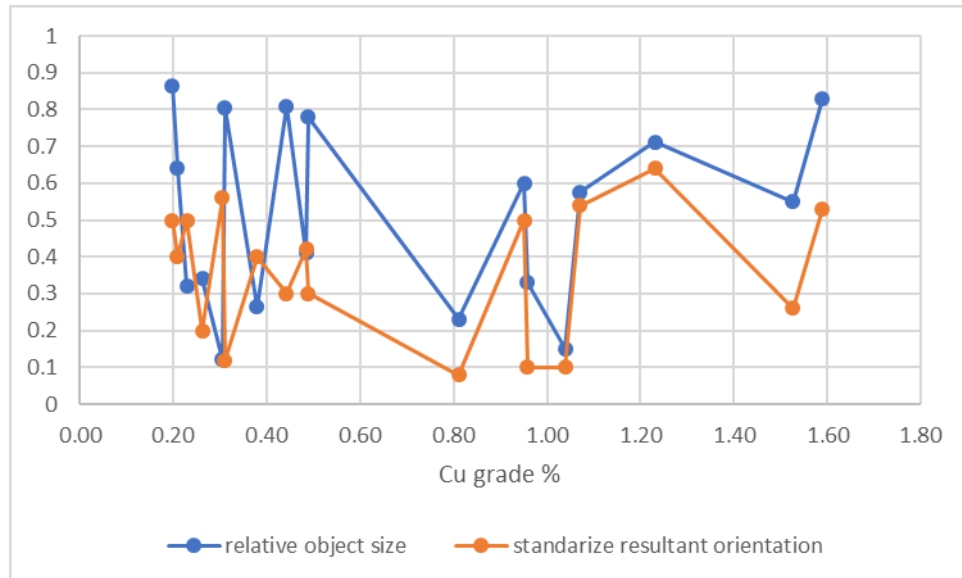
Figure 25. Scatter plot of relative object size and standardize resultant of tourmaline bearing rock compare to copper content

Figure 25 shows that the graph of relative object size and standardize resultant of tourmaline bearing rock versus copper content have an interesting pattern. The graph of relative object size and standardize resultant have a similar pattern with increasing copper content. This process can occur as the high copper content corresponds to the porphyritic texture with vein texture. Further research is needed to investigate another factor that may influence this pattern.

According to the data integration result, tourmaline mineral is an indicator of high copper content. About 18 rock samples have 0.69% Cu than non-tourmaline rock has 0.38% Cu. Tourmaline texture measurement such as flattening and convexity do not have relation with the copper grade based on the statistic result. The convexity of tourmaline mineral has R^2 value 0.03, which indicate low correlation between convexity and copper grade. The flattening parameter of tourmaline mineral has R^2 value 0.01 which also indicate low correlation between flattening and copper grade. Even though the flattening and convexity have low correlation with copper content, the flattening value can be used to determine vein shape and spot/disseminated shape. High content of copper corresponds to vein shape. Convexity parameter can be used to differentiate shape crystal. The subhedral and anhedral shape correspond to high copper content.

The relative object size for all milled pebble sample has value 0.02 that indicates low correlation with copper concentration. However, relative object can be used to highlight high copper concentration which has porphyritic texture. Standardize resultant is determined by orientation clast/phenocryst or vein of rock. Based on statistical data, clast orientation has low correlation with copper content as the R^2 value of standardize resultant is 0.02. The random direction of clast/phenocryst refers to high copper content.

As the ore texture measurement parameter shows low correlation with the copper content, these parameters are independent with the copper content on the rock sample.

6. CONCLUSION AND RECOMMENDATION

6.1. Conclusion

Ore texture of 43 milled pebbles was analyzed using high-resolution hyperspectral images in the SWIR wavelength range and compared with copper concentration.

According to the research study the following conclusion can be drawn for the Los Bronces milled pebbles sample:

- The visual interpretation of 43 milled pebbles was classified to 5 groups based on the texture, crystal color, crystal size, matrix color, and matrix size. Phaneritic, porphyritic, and aphanitic texture is found from the visual interpretation. Vein and disseminated texture also present on the rock sample.

- The mineral map resulted from hyperspectral images illustrates the distribution of mineral spatially and reflects rock texture. The mineral map is capable of providing information for texture analysis of the milled pebble rock. The mineral map generated a similar result as visual interpretation where the phaneritic, porphyritic, and aphanitic texture present on the sample. Vein and disseminated texture also can be found on the rock sample.

- Hyperspectral images in the SWIR region can identify mineral in the milled pebble sample. Hyperspectral imagery can determine AlOH, FeOH, MgOH and CO_3 mineral group.

- Decision tree classification can be used to generate a mineral map from hyperspectral images in the SWIR range. using various kind of source such as, illite crystallinity, kaolinite ratio, wavelength map, decision tree classification can generate mineral map.

- Rock texture measurement is able to determine the shape of phenocryst, vein structure with spot shape, clast distribution and phenocryst orientation. The flattening parameter can be differentiated shape of vein structure and spot; convexity can be used to differentiate crystal shape. Relative object can be used to determine distribution crystal. Standardize resultant can be used to determine preferred or random orientation of crystal.

- Tourmaline mineral was an indicator of high concentration of copper as seen in the 18 samples with Tourmaline. Tourmaline veins with low flattening also had high copper content.

- Cu grade has low correlation with flattening, convexity, standardize resultant and relative object size based on the statistical data. The convexity of tourmaline mineral has R2 value 0.03, which indicate low correlation between convexity and copper grade. The flattening parameter of tourmaline mineral has R^2 value 0.01 which also indicate low correlation between flattening and copper grade. The relative object size for all milled pebble sample has value 0.02 that indicates low correlation with copper concentration. Based on statistical data, clast orientation has low correlation with copper content as the R^2 value of standardize resultant is 0.02.

6.2. Recommendation

Further research should be conducted to observe other texture from hyperspectral image. In Los Bronces porphyry Cu milled pebbles has veinlet and disseminated ore texture. Other deposits have different type and characteristic, it will be interesting to analyze it, such as comb texture, crustiform, colloform, stratiform and may show patterns not observed within the samples available in this study. Based on this study, the relative object size and standardize resultant versus copper content have a similar pattern. Further study may be needed to find other factors that affect this unique pattern.

Shaper script can be further developed to improve the accuracy of texture measurement, and also increase the object size threshold, so fine grained mineral/clast can be recognized.

7. LIST OF REFERENCES

Agus, A. J. L. (2011). *Mapping white mica in milled porphyry copper pebbles using hyperspectral imagery: An exploratory study. Geo-infromation science and earth observation.* University of Twente. Retrieved from http://adlib.itc.utwente.nl/brief.aspx

Allaby, M. (2013). *A Dictionary of Geology and Earth Sciences* (Fourth edi). Oxford: Oxford University Press.

Arndt, N., Ganino, C., & Kesler, S. (2012). *Metals and Society* (Second Edi). Paris: Springer International Publishing AG. https://doi.org/10.1007/978-3-642-22996-1

Bakker, W. H. (2012). HypPy User Manual. *ITC - University of Twente.* Retrieved from http://www.itc.nl/personal/bakker/hyppy.html

Baksheev, I. A., Yu Prokof'ev, V., Zaraisky, G. P., Chitalin, A. F., Yapaskurt, V. O., Nikolaev, Y. N., … Kononov, O. V. (2012). Tourmaline as a prospecting guide for the porphyry-style deposits. *European Journal of Mineralogy*, *24*(6), 957–979. https://doi.org/10.1127/0935-1221/2012/0024-2241

Barrie, C. D., Cook, N. J., & Boyle, A. P. (2010). Textural variation in the pyrite-rich ore deposits of the Røros district, Trondheim Region, Norway: Implications for pyrite deformation mechanisms. *Mineralium Deposita*, *45*(1), 51–68. https://doi.org/10.1007/s00126-009-0261-3

Clark, R. N., King, T. V. V, Klejwa, M., Swayze, G. A., & Vergo, N. (1990). High spectral resolution reflectance spectroscopy of minerals. *Journal of Geophysical Research: Solid Earth*, *95*(B8), 12653–12680. https://doi.org/10.1029/JB095iB08p12653

Corbett, G. J., & Leach, T. M. (1998). Southwest Pacific rim gold–copper systems: structure, alteration and mineralization. *Society of Economic Geologists*, *Special Pu*(May 1997), 236.

Craig, J. R., & Vaughan, D. J. (1994). *Ore Microscopy and Ore Petrography. Minerals Engineering.* https://doi.org/10.1016/S0892-6875(96)90069-2

Dalm, M., Buxton, M. W. N., & van Ruitenbeek, F. J. A. (2017). Discriminating ore and waste in a porphyry copper deposit using short-wavelength infrared (SWIR) hyperspectral imagery. *Minerals Engineering*, *105*, 10–18. https://doi.org/10.1016/J.MINENG.2016.12.013

Frikken, P. H., Cooke, D. R., Walshe, J. L., Archibald, D., Skarmeta, J., Serrano, L., & Vargas, R. (2005). Mineralogical and isotopic zonation in the Sur-Sur tourmaline breccia, Río Blanco-Los Bronces Cu-Mo deposit, Chile: Implications for ore genesis. *Economic Geology*, *100*(5), 935–961. https://doi.org/10.2113/gsecongeo.100.5.935

Hauff, P. (1983). *An overview of VIS-NIR-SWIR field spectroscopy as applied to precious metals exploration. Arvada, Colorado: Spectral International Inc* (Vol. 80001).

Higgins, M. D. (2006). *Quantitative textural measurements in igneous and metamorphic petrology. Quantitative Textural Measurements in Igneous and Metamorphic Petrology.* https://doi.org/10.1017/CBO9780511535574

Ineson, P. R. (1989). *Introduction to Practical Ore Microscopy (Longman Earth Science Series).* (P. J. Z. Zussma & M. W. S., Eds.) (1 edition). New York: Routledge.

Laakso, K., Middleton, M., Heinig, T., Bärs, R., & Lintinen, P. (2018). Assessing the ability to combine hyperspectral imaging (HSI) data with Mineral Liberation Analyzer (MLA) data to characterize phosphate rocks. *International Journal of Applied Earth Observation and Geoinformation*, *69*, 1–12. https://doi.org/10.1016/J.JAG.2018.02.018

Mathieu, M., Roy, R., Launeau, P., Cathelineau, M., & Quirt, D. (2017). Alteration mapping on drill cores using a HySpex SWIR-320m hyperspectral camera: Application to the exploration of an unconformity-related uranium deposit (Saskatchewan, Canada) ☆. *Journal of Geochemical Exploration*, *172*, 71–88. https://doi.org/10.1016/j.gexplo.2016.09.008

Northey, S. A., Mudd, G. M., Werner, T. T., Jowitt, S. M., Haque, N., Yellishetty, M., & Weng, Z. (2017). The exposure of global base metal resources to water criticality, scarcity and climate change. *Global Environmental Change*, *44*, 109–124. https://doi.org/10.1016/J.GLOENVCHA.2017.04.004

Pirajno, F. (2009). *Hydrothermal processes and mineral systems. Hydrothermal Processes and Mineral Systems* (first). Perth: Springer International Publishing. https://doi.org/10.1007/978-1-4020-8613-7

Pontual, S., Merry, N., & Gamson, P. (1997). *Spectral Analysis Guides for Mineral Exploration: Vol 2 - Practical*

Applications. AusSpec International Pty.

Robb, L. (2005). *Introduction To Ore-Forming Processes,. Blackwell Publishing* (First, Vol. 1). Oxford: Blackwell Publishing company. https://doi.org/10.2138/am.2005.426

Sillitoe, R. H. (2010). Porphyry copper systems. *Economic Geology*, *105*(1), 3–41. https://doi.org/10.2113/gsecongeo.105.1.3

Skarmeta, J., & Cooke, D. R. (2015). Structural Evolution of the Rio Blanco-Los Bronces District, Andes of Central Chile: Controls on Stratigraphy, Magmatism, and Mineralization, 1995–2023.

Skewes, M. A., Holmgren, Æ. C., & Stern, C. R. (2003). The Donoso copper-rich , tourmaline-bearing breccia pipe in central Chile : petrologic , fluid inclusion and stable isotope evidence for an origin from magmatic fluids, 2–21. https://doi.org/10.1007/s00126-002-0264-9

SPECIM. (2015). SisuCHEMA: spectral camera, (384).

Taylor, R. (2009). *Ore Textures Recognition and Interpretation* (first). Berlin: Springer International Publishing. https://doi.org/10.1007/978-3-642-01783-4

Tripathy, D. P., & Reddy, K. G. R. (2017). Multispectral and joint colour-texture feature extraction for ore-gangue separation. *Pattern Recognition and Image Analysis*, *27*(2), 338–348. https://doi.org/10.1134/S1054661816040179

Van Ruitenbeek, F. J. A., Bakker, W. H., Van Der Werff, H. M. A., Zegers, T. E., Oosthoek, J. H. P., Omer, Z. A., … Van Der Meer, F. D. (2014). Mapping the wavelength position of deepest absorption features to explore mineral diversity in hyperspectral images. *Planetary and Space Science*, *101*, 108–117. https://doi.org/10.1016/j.pss.2014.06.009

van Ruitenbeek, F. J. A., van der Werff, H. M. A., Bakker, W. H., van der Meer, F. D., & Hein, K. A. A. (2019). Measuring rock microstructure in hyperspectral mineral maps. *Remote Sensing of Environment*, *220*(October 2018), 94–109. https://doi.org/10.1016/j.rse.2018.10.030

Warnaars, F. W., Holmgren, C., & Barassi, S. (1985). Porphyry copper and tourmaline breccias at Los-Bronces-Rio-Blanco, Chile. *Economic Geology*, *80*(6), 1544–1565. https://doi.org/10.2113/gsecongeo.80.6.1544

Yousefia, S. J., Ranjbar, H., Alirezaeics, S., Dargahid, S., & Lentze, D. R. (2018). Comparison of Hydrothermal Alteration Patterns Associated with Porphyry Cu Deposits hosted by Granitoids and Intermediate-mafic Volcanic rocks, Kerman Magmatic Arc, Iran: application of geological, mineralogical and remote sensing data. *Journal of African Earth Sciences*, *142*, 112–123. https://doi.org/10.1016/j.jafrearsci.2018.03.005

Zhang, X., Treitz, P. M., Chen, D., Quan, C., Shi, L., & Li, X. (2017). Mapping mangrove forests using multi-tidal remotely-sensed data and a decision-tree-based procedure. *International Journal of Applied Earth Observation and Geoinformation*, *62*(June), 201–214. https://doi.org/10.1016/j.jag.2017.06.010

Appendix

Appendix 1. figure RGB photo, mineral map and image object edge with Cu concentration from all sample
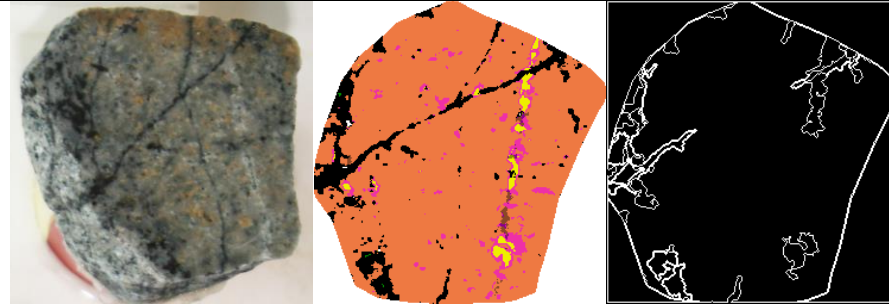
Sample 76, 1.59% Cu
Sample 10, 1.53% Cu
Sample 107, 1.42% Cu
Sample 92, 1.23% Cu
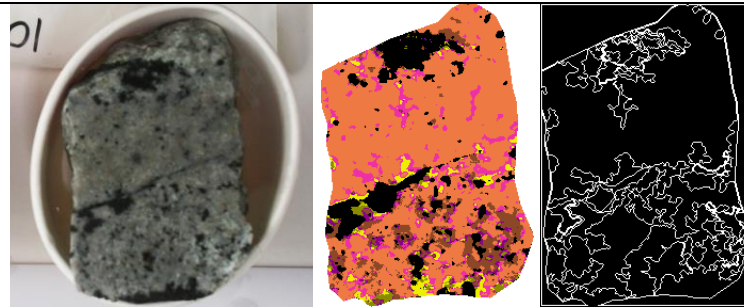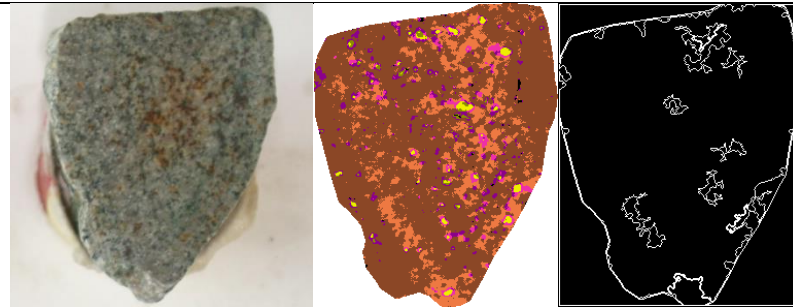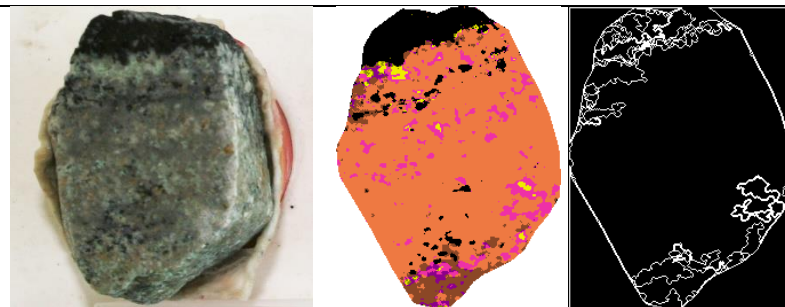
Legend

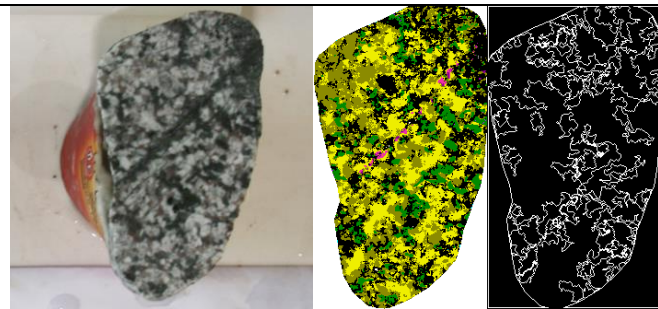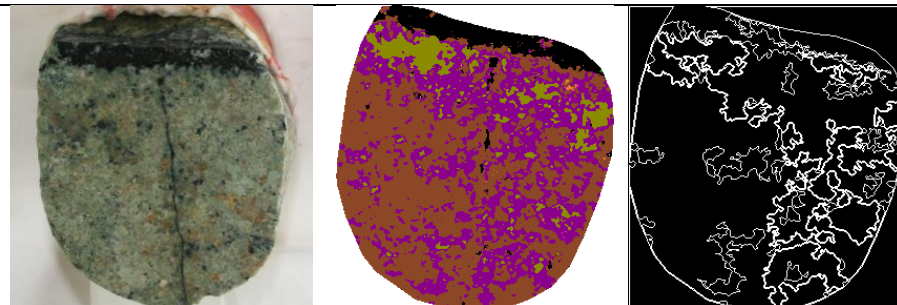|			
Illite <2207 nm	Illite >2207 nm	Illite-kaolinite	Fe chlorite
Muscovite <2207 nm	Muscovite >2207 nm	kaolinite	Mg Chlorite
HX Illite <2207 nm	HX Illite >2207 nm	tourmaline	other

Sample 148a, 1.07% Cu
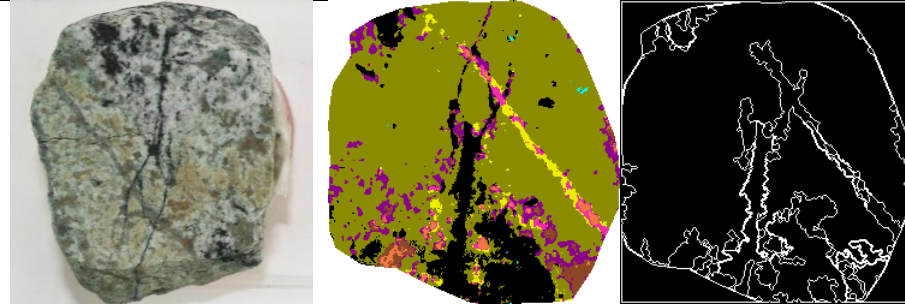
Sample 43, 1.04% Cu
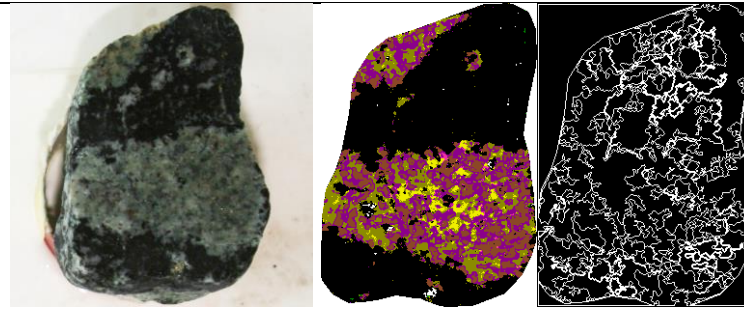
Sample 60, 0.96% Cu
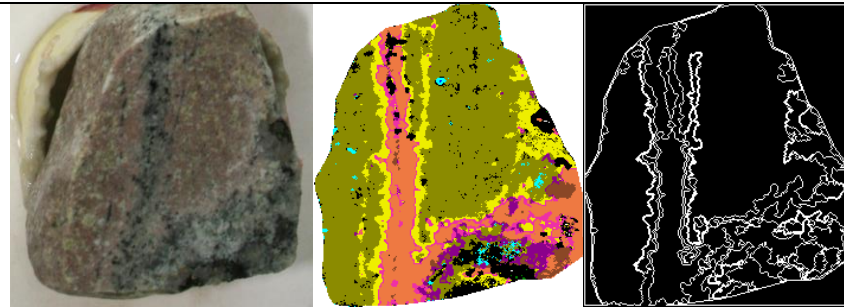
Sample 62, 0.95% Cu
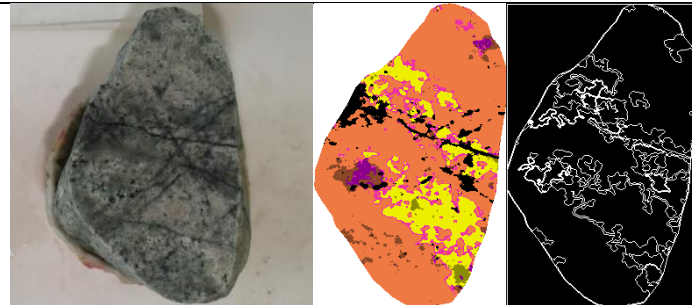
Legend

Illite <2207 nm	Illite >2207 nm	Illite-kaolinite	Fe chlorite
Muscovite <2207 nm	Muscovite >2207 nm	kaolinite	Mg Chlorite
HX Illite <2207 nm	HX Illite >2207 nm	tourmaline	other

Sample 47, 0.81% Cu
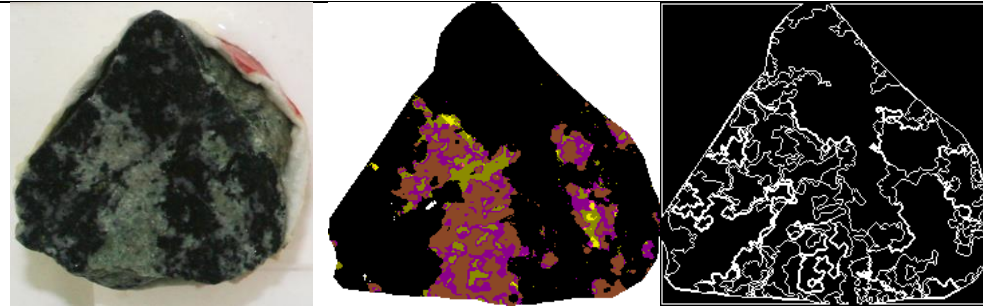
Sample 117, 0.62% Cu
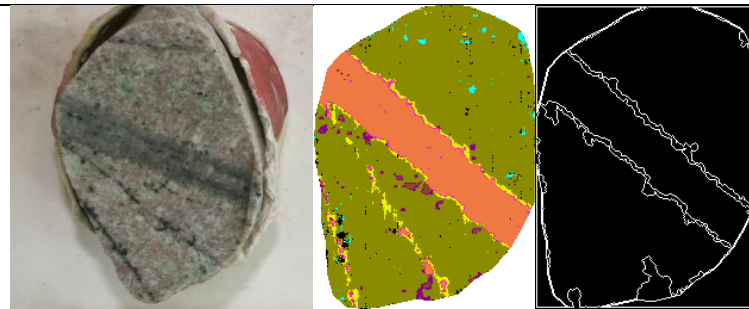
Sample 101, 0.62% Cu
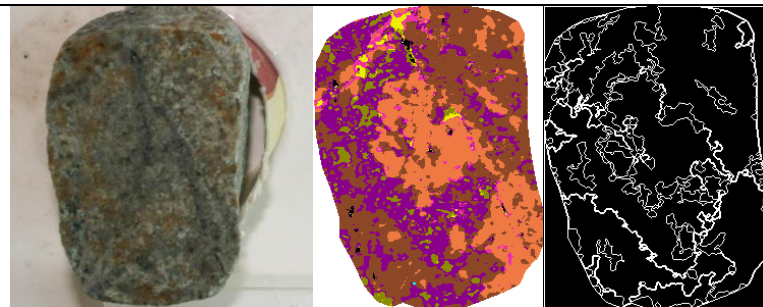
Sample 35, 0.56% Cu
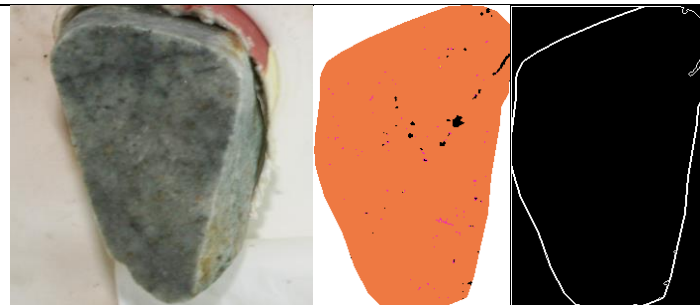
Legend

Illite <2207 nm	Illite >2207 nm	Illite-kaolinite	Fe chlorite
Muscovite <2207 nm	Muscovite >2207 nm	kaolinite	Mg Chlorite
HX Illite <2207 nm	HX Illite >2207 nm	tourmaline	other

Sample 132, 0.49% Cu

Sample 2, 0.48% Cu
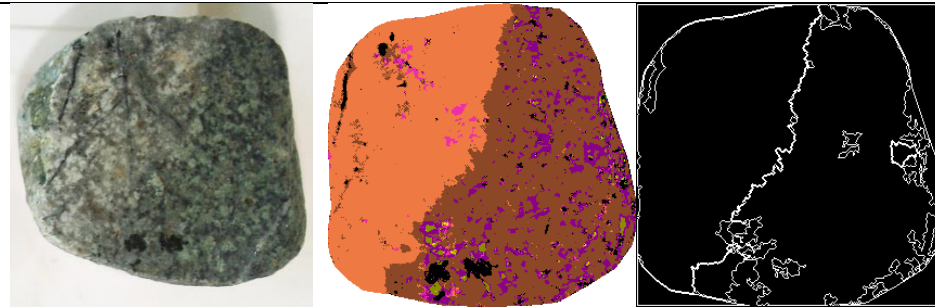
Sample 125, 0.48% Cu
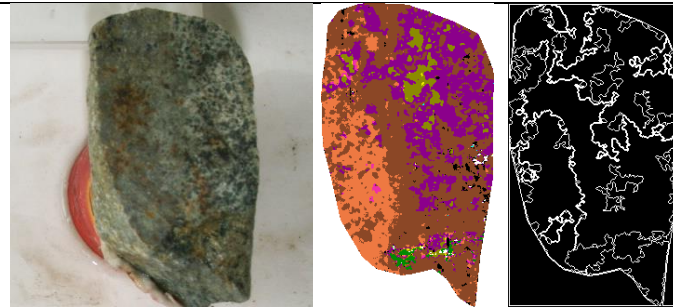
Sample 31, 0.47% Cu
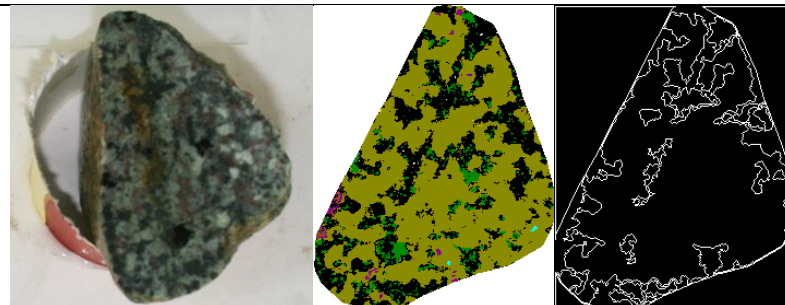
Legend

Illite <2207 nm	Illite >2207 nm	Illite-kaolinite	Fe chlorite
Muscovite <2207 nm	Muscovite >2207 nm	kaolinite	Mg Chlorite
HX Illite <2207 nm	HX Illite >2207 nm	tourmaline	other
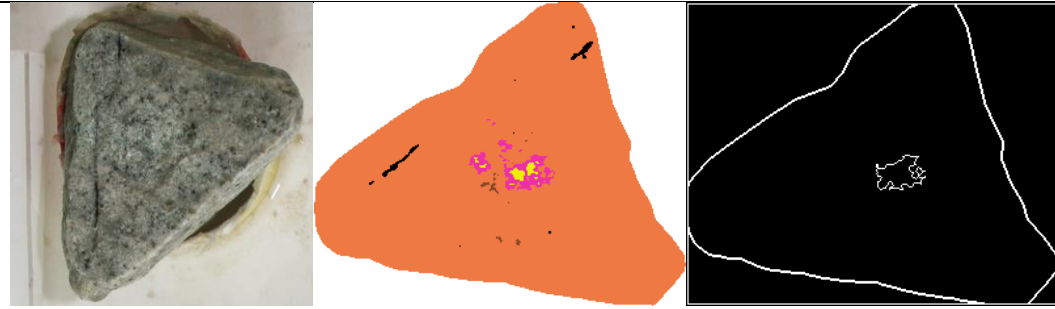
Sample 15, 0.47% Cu
Sample 40, 0.44% Cu
Sample 111, 0.44% Cu
Sample 116, 0.38% Cu
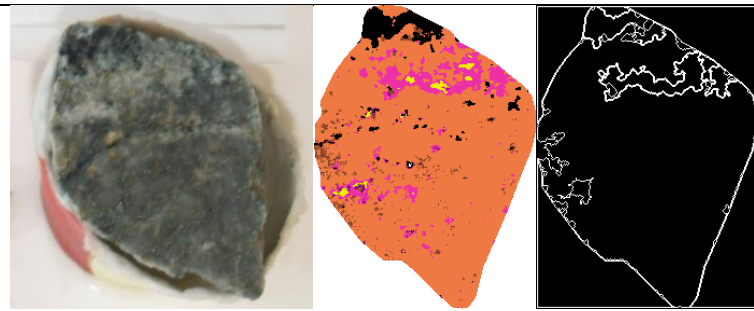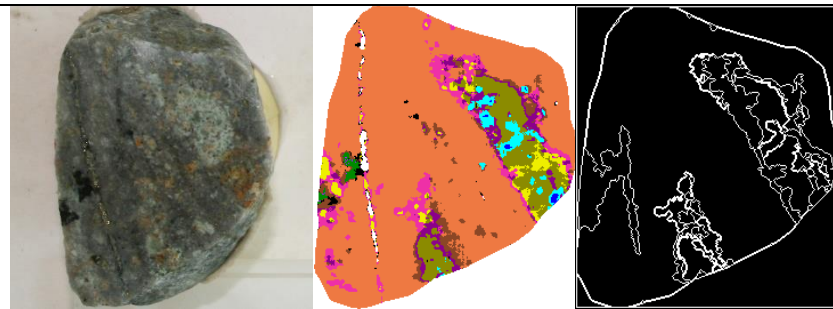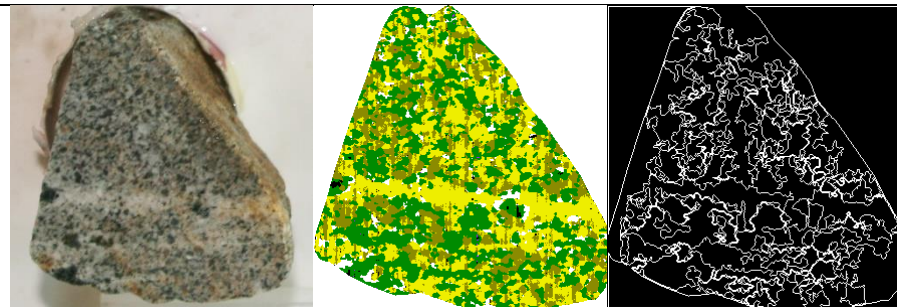
Legend

Illite <2207 nm (yellow)	Illite >2207 nm (olive)	Illite-kaolinite (cyan)	Fe chlorite (green)
Muscovite <2207 nm (orange)	Muscovite >2207 nm (brown)	kaolinite (blue)	Mg Chlorite (dark green)
HX Illite <2207 nm (magenta)	HX Illite >2207 nm (purple)	tourmaline (black)	other (violet)
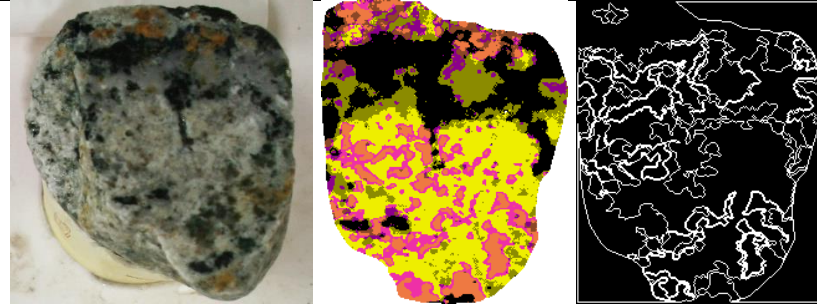
Sample 106, 0.38% Cu
Sample 145, 0.38% Cu
Sample 65, 0.36% Cu
Sample 95, 0.36% Cu
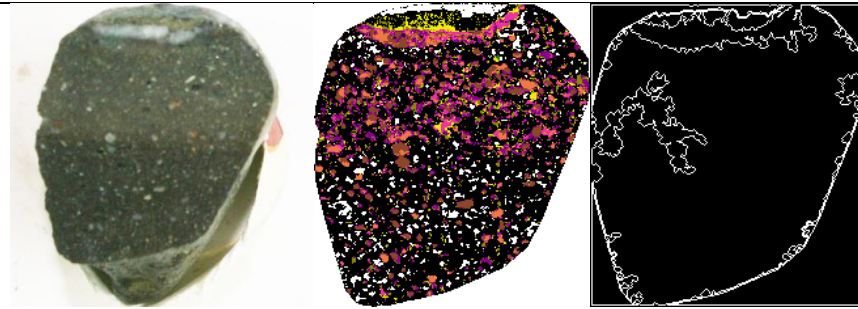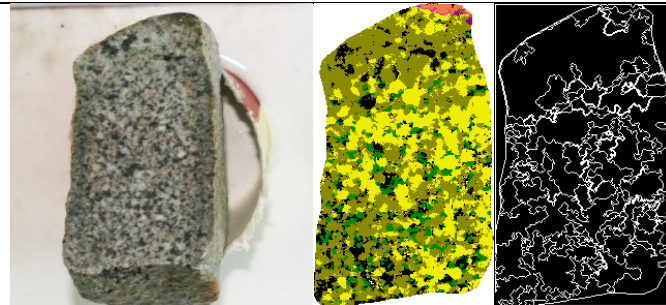
Legend

Illite <2207 nm	Illite >2207 nm	Illite-kaolinite	Fe chlorite
Muscovite <2207 nm	Muscovite >2207 nm	kaolinite	Mg Chlorite
HX Illite <2207 nm	HX Illite >2207 nm	tourmaline	other
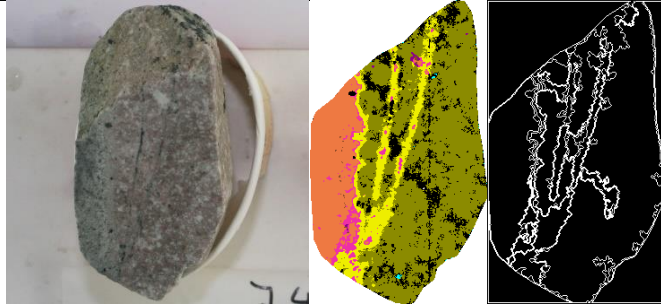
Sample 74, 0.35% Cu
Sample 128, 0.34% Cu
Sample 68, 0.34% Cu
Sample 97, 0.31% Cu
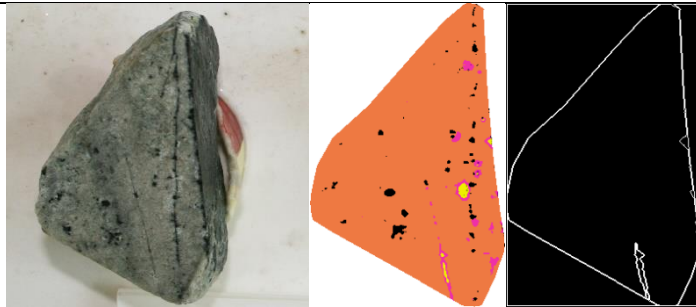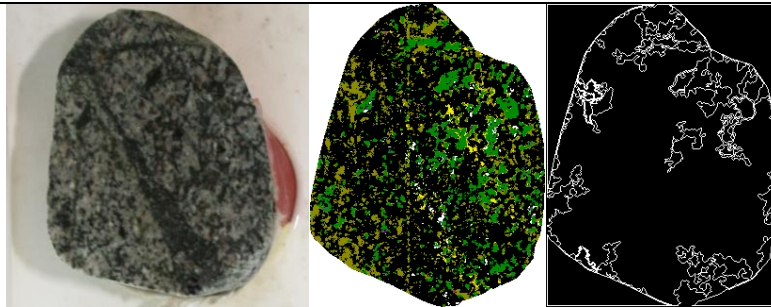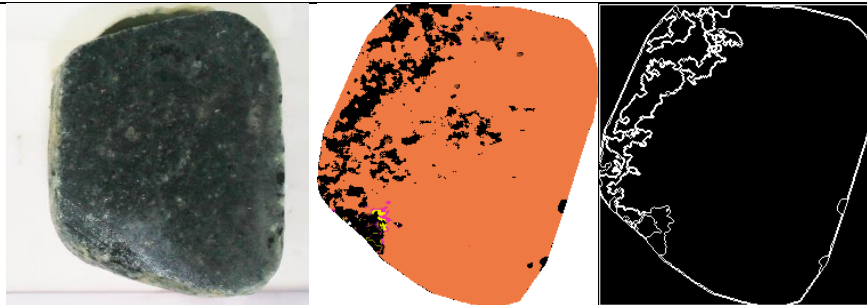
Legend

Illite <2207 nm	Illite >2207 nm	Illite-kaolinite	Fe chlorite
Muscovite <2207 nm	Muscovite >2207 nm	kaolinite	Mg Chlorite
HX Illite <2207 nm	HX Illite >2207 nm	tourmaline	other
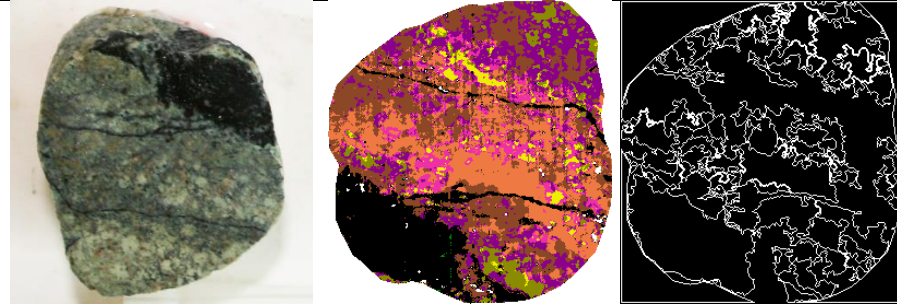
Sample 119, 0.31% Cu
Sample 8, 0.30% Cu
Sample 9, 0.27% Cu
Sample 42, 0.26% Cu
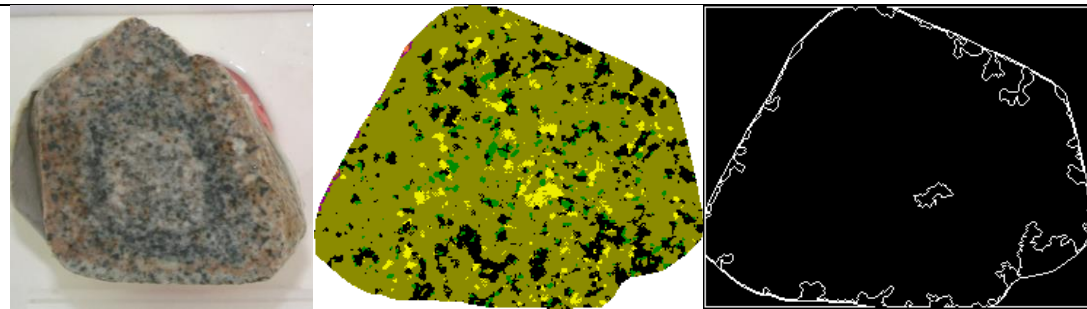
Legend

Illite <2207 nm	Illite >2207 nm	Illite-kaolinite	Fe chlorite
Muscovite <2207 nm	Muscovite >2207 nm	kaolinite	Mg Chlorite
HX Illite <2207 nm	HX Illite >2207 nm	tourmaline	other

Sample 4, 0.26% Cu
Sample 137, 0.23% Cu
Sample 113, 0.21% Cu
Sample 110, 0.20% Cu
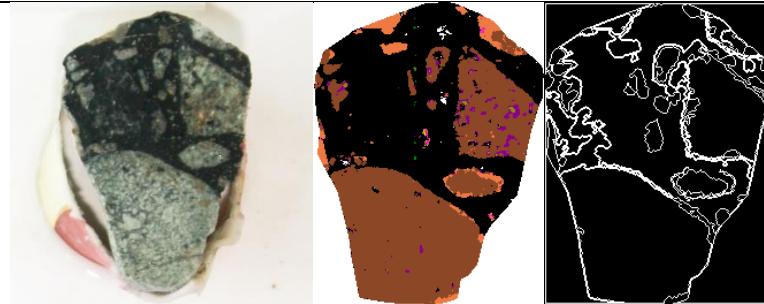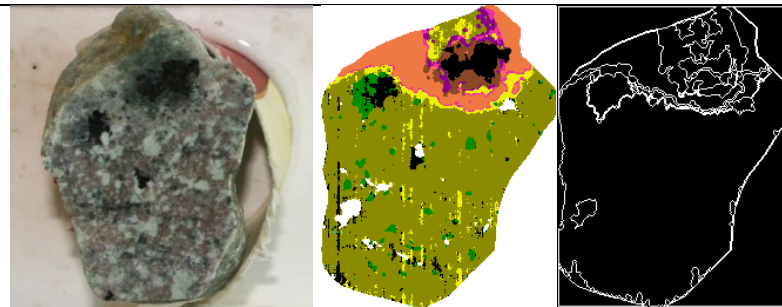
Legend

▮ Illite <2207 nm	▮ Illite >2207 nm	▮ Illite-kaolinite	▮ Fe chlorite
▮ Muscovite <2207 nm	▮ Muscovite >2207 nm	▮ kaolinite	▮ Mg Chlorite
▮ HX Illite <2207 nm	▮ HX Illite >2207 nm	▮ tourmaline	▮ other

Sample 5, 0.19% Cu

Sample 22, 0.17% Cu
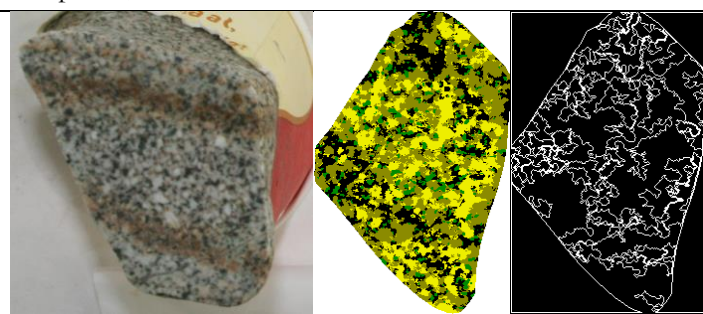
Sample 44, 0.17% Cu
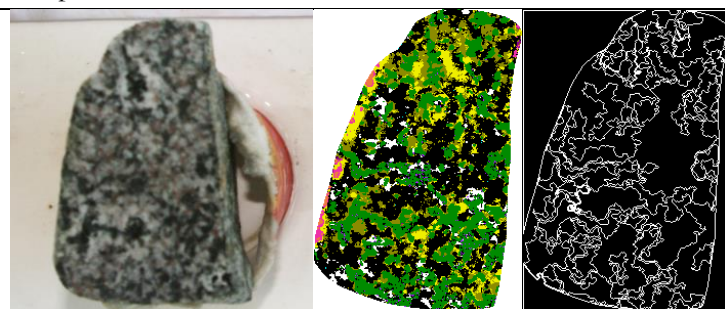
Sample 6, 0.15% Cu
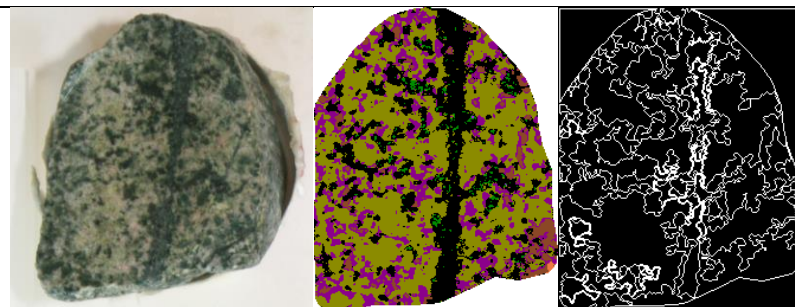
Legend

Colour	Mineral	Colour	Mineral	Colour	Mineral	Colour	Mineral
yellow	Illite <2207 nm	olive	Illite >2207 nm	cyan	Illite-kaolinite	bright green	Fe chlorite
orange	Muscovite <2207 nm	brown	Muscovite >2207 nm	blue	kaolinite	dark green	Mg Chlorite
pink	HX Illite <2207 nm	purple	HX Illite >2207 nm	black	tourmaline	violet	other

Sample 61, 0.14% Cu

Sample 133, 0.13% Cu

Sample 39, 0.11% Cu

Legend			
Illite <2207 nm	Illite >2207 nm	Illite-kaolinite	Fe chlorite
Muscovite <2207 nm	Muscovite >2207 nm	kaolinite	Mg Chlorite
HX Illite <2207 nm	HX Illite >2207 nm	tourmaline	other

Appendix 2. table of homogeneity, relative object, standardize resultant and visual interpretation group from all rock

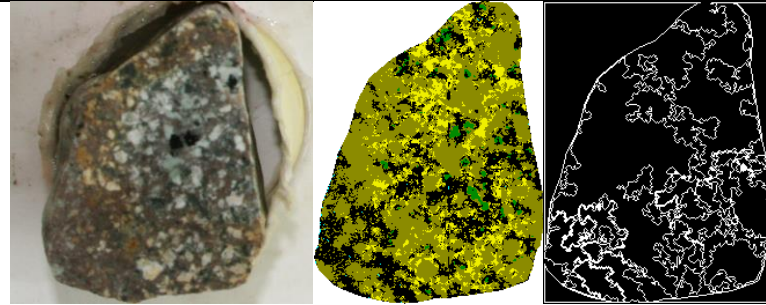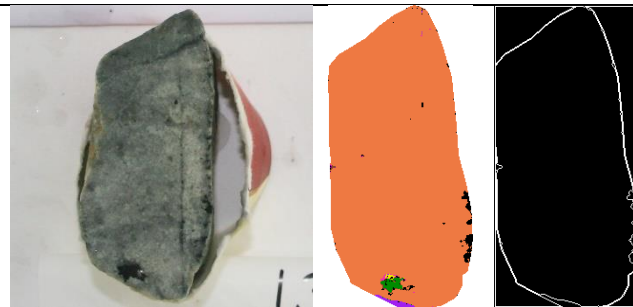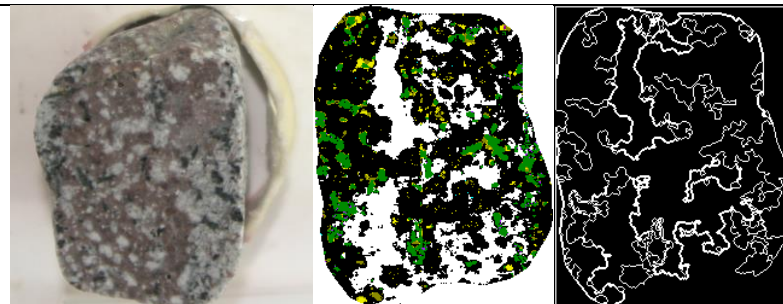| No sample	Cu grade	Homogeneity	Relative object size	Standarize resultant	Visual interpreetation group
76	1.59	1.00	0.83	0.53	c
10	1.53	0.95	0.55	0.26	c
107	1.42	1.00	0.73	0.04	d
92	1.23	0.88	0.71	0.64	c
148	1.07	0.88	0.57	0.54	c
43	1.04	0.32	0.15	0.1	c
60	0.96	0.44	0.33	0.1	d
62	0.95	1.00	0.6	0.5	c
47	0.81	0.42	0.23	0.08	c
117	0.62	0.44	0.39	1.00	d
101	0.62	0.32	0.18	0.35	c
35	0.56	1.00	1	1	a
132	0.49	1.00	0.78	0.3	c
2	0.48	0.58	0.41	0.42	c
125	0.48	0.73	0.34	0.32	c
31	0.47	0.97	0.61	0.16	e
15	0.47	1.00	0.99	1	c
40	0.44	1.00	0.81	0.3	c
111	0.44	1.00	0.71	0.62	c
116	0.38	0.28	0.26	0.22	c
145	0.38	1.00	0.60	0.78	c
106	0.38	0.52	0.26	0.40	c
65	0.36	1.00	0.65	0.8	c
95	0.36	0.28	0.16	0.11	c
74	0.35	0.60	0.42	0.6	d
128	0.34	1.00	1.0	1.00	c
68	0.34	1.00	0.6	0.3	c
97	0.31	0.93	0.80	0.12	a
119	0.31	0.15	0.12	0.56	c
8	0.30	1.00	0.75	1	c
9	0.27	0.13	0.07	0.15	e
42	0.26	0.52	0.34	0.2	c
4	0.26	1.00	0.66	0.19	e
137	0.23	0.67	0.32	0.5	b
113	0.21	0.90	0.64	0.40	c
110	0.20	1.00	0.86	0.5	d
5	0.19	0.53	0.28	0.14	c
22	0.17	0.14	0.07	0.07	e
44	0.17	0.39	0.2	0.29	e
6	0.15	0.24	0.14	0.19	c
61	0.14	0.50	0.26	0.23	e
133	0.13	1.00	1	1	a
39	0.11	1.00	0.52	0.3	c

Appendix 3. table of shape parameter from tourmaline sample

No sample	X	Y	O_Area	E_Angle	Compact	Convex	Cookie	Flattening	Hollowness	Cu grade	Group
76	190.7	54.3	409	61	0.18	0.82	0.13	0.22	0.53	1.59	ore
76	53.1	229	675	148	0.21	0.61	0.06	0.47	0.71	1.59	ore
76	24.6	116.3	1644	10	0.07	0.53	0.19	0.48	0.34	1.59	ore
10	65.1	177.2	927	59	0.29	0.83	0.11	0.33	0.68	1.53	ore
10	22.9	200.3	732	176	0.44	0.81	0.09	0.82	0.78	1.53	ore
92	74.8	21.6	1774	76	0.04	0.40	0.10	0.35	0.44	1.23	ore
148	50	23.6	498	169	0.59	0.92	0.09	0.71	0.84	1.07	ore
148	133.7	206.8	5630	156	0.09	0.47	0.12	0.60	0.59	1.07	ore
43	78.8	280.7	8623	100	0.26	0.74	0.17	0.30	0.74	1.04	ore
43	136.7	91.9	21016	59	0.30	0.67	0.11	0.56	0.82	1.04	ore
60	193.1	98.8	285	145	0.64	0.95	0.07	0.69	0.87	0.96	ore
60	127.2	240.8	293	76	0.35	0.83	0.09	0.30	0.82	0.96	ore
60	130.3	211.4	275	53	0.28	0.72	0.08	0.50	0.70	0.96	ore
60	162.2	220.7	626	119	0.22	0.66	0.08	0.40	0.70	0.96	ore
62	173.8	204.1	304	136	0.41	0.84	0.09	0.61	0.78	0.95	ore
62	174.5	164.5	316	107	0.12	0.81	0.15	0.14	0.47	0.95	ore
62	119.5	143.8	226	109	0.11	0.70	0.01	0.34	0.38	0.95	ore
62	54.4	120	1241	84	0.11	0.49	0.09	0.79	0.60	0.95	ore
47	159.4	113.4	18506	149	0.33	0.75	0.10	0.45	0.74	0.81	ore
47	46.4	161.4	7594	10	0.25	0.64	0.13	0.61	0.77	0.81	ore
132	172.3	111.3	1534	177	0.14	0.86	0.10	0.11	0.64	0.49	ore
132	91.5	14.2	678	78	0.13	0.56	0.12	0.35	0.59	0.49	ore
132	108.2	60.3	645	120	0.12	0.52	0.07	0.74	0.56	0.49	ore
132	104.2	155	3759	173	0.08	0.43	0.19	0.42	0.53	0.49	ore
2	138.1	243.5	273	100	0.14	0.54	0.06	0.59	0.61	0.48	ore
40	79	19.9	1178	94	0.17	0.64	0.09	0.39	0.54	0.44	ore
106	7	88.5	474	1	0.37	0.84	0.08	0.28	0.84	0.38	waste
106	106.2	64.3	7804	100	0.06	0.41	0.18	0.41	0.47	0.38	waste
97	40.3	194.2	741	130	0.19	0.66	0.14	0.42	0.68	0.31	waste
97	77	16.3	886	60	0.12	0.61	0.09	0.35	0.54	0.31	waste
97	91	53.7	480	63	0.17	0.61	0.09	0.53	0.59	0.31	waste
97	104.8	25.2	401	125	0.15	0.57	0.05	0.47	0.61	0.31	waste
97	34.6	103.9	2180	26	0.05	0.45	0.19	0.23	0.47	0.31	waste
119	162.2	267.7	391	112	0.29	0.82	0.12	0.40	0.72	0.31	waste
119	68	213.5	8609	117	0.14	0.55	0.28	0.62	0.60	0.31	waste
42	147.6	30.5	3614	104	0.13	0.76	0.17	0.10	0.72	0.26	waste
137	89.9	88.9	18178	128	0.21	0.61	0.12	0.90	0.62	0.23	waste
113	132.2	48	1016	77	0.30	0.73	0.10	0.46	0.70	0.21	waste
113	51.4	72.8	402	46	0.26	0.65	0.13	0.71	0.70	0.21	waste
110	114.5	62	764	26	0.14	0.78	0.20	0.16	0.58	0.20	waste
110	87.7	54.1	483	41	0.17	0.71	0.14	0.24	0.69	0.20	waste

Appendix 4. confusion matrices of decision tree classification images

Sample 4

	Illite SW	muscovite SW	tourmaline	chlorite	total
Illite SW	14	0	1	0	15
muscovite SW	0	1	0	0	1
tourmaline	0	0	0	3	3
chlorite	0	0	0	1	1
total	14	1	1	4	20

overall accuracy : 80%
Kappa score   :0.56

Sample 6

	chlorite	tourmaline	HX illite LW	illite LW	total
chlorite	0	4	0	0	4
tourmaline	0	0	0	0	0
HX illite LW	0	0	8	0	8
illite LW	0	2	0	6	8
total	0	6	8	6	20

overall accuracy : 70%
Kappa score   :0.53

Sample 62

	muscoviteSW	tourmaline	HX illite SW	illite SW	total
muscovite sw	13	1	0	0	14
tourmaline	0	1	0	0	1
HX illite SW	0	0	2	0	2
illite SW	0	0	0	3	3
total	13	2	2	3	20

overall accuracy : 95%
Kappa score   :0.9

Sample 137

	muscovite lw	tourmaline	total
muscovite lw	10	1	11
tourmaline	0	9	9
total	10	10	20

overall accuracy : 95%
Kappa score   :0.9

Appendix 5 table of XRD, XRF and thin section of milled pebbles

no sample	Cu grade %	XRD	Thin section
2	0.48	quartz, muscovite, pyrite or hematite, titanite	
4	0.26	quartz, plagioclase (albite), k feldspar (orthoclase), chlorite (clinochore), muscovite	
5	0.19		quartz, sericite, heamtite, magnetite, pyrite, tourmaline, rutile, chalcopyrite,digenite
6	0.15	quartz, chlorite, muscovite, k feldspar(sanidine)	
8	0.30	quartz, plagioclase (albite), k feldspar (orthoclase), chlorite (clinochore), muscovite	
9	0.27	quartz, plagioclase (albite), chlorite (chlorite-serpentin), muscovite	
10	1.53	quartz, muscovite, chacopyrite, pyrite	
15	0.47		quartz, mica, pyrite, tourmaline, rutile, chalcopyrite, digenite
22	0.17	quartz, plagioclase(albite), chlorite (cliniclore), muscovite, k feldspar(microcline), rutile	
31	0.47		
35	0.56	quatz, muscovite, pyridte or hematite, chalcopyrite, tourmaline, titanite	
39	0.11	quartz, plagioclase(albite), k-feldsaor(orthoclase), chlorite(clinichlore), biotite	
40	0.44		
42	0.26		quartz, k-feldspar, hematite, pyrite, tourmaline, rutile, chalcopyrite, digenite
43	1.04	quartz, chalcopyrite, muscovite, hematite, orthoferrosilite	
44	0.17		quartz, plagioclase, k-feldsoar, chlorite, biotite, chalcopyrite, digenite, covellite, magneite, rutile
47	0.81		quartz, muscovite, sericite, tourmaline, chalcopyrite, chalcocotedigenite
60	0.96	quartz, k-feldsapr, plagioclase, muscovite, chalcopyrite, tourmaline, rutile, chalcocite	
61	0.14		quatz, plagioclase, chlorite, sericite, chalcopyrite, bornite, digenite
62	0.95	quartz, muscovite, k-feldspar, chalcopyrite	
65	0.36	quartz, muscovite, pyrite	
68	0.34	quartz, muscovite, hematite, kaolinite	
74	0.35		quartz, muscovite, sericite, pyrite, tourmaline, rutile, chalcopyrite, chalcocite, covellite, digenite
76	1.59	quartz, muscovite, pyrite	
92	1.23		
95	0.36		quartz, chlorite, muscovite, sericite, magnetite, bornite, chalcocite
97	0.31	quartz, muscovite, tourmaline	
101	0.62	quartz, muscovite, pyrite, or heamtite, titanite	
106	0.38	quartz, tourmaline, k-feldspar, plagioclase, muscovite, titanite, chalcocite	
107	1.42		chalcocite, muscovite, titanite, molybdenite, actinolite, chalcopyrite
110	0.20		k-feldspar, plagioclase, quartz, chlotite, muscovite, chalcopyrite, covellite, tennanite, tetrahydrite, rutile
111	0.44		
113	0.21		
116	0.38		
117	0.62		
119	0.31		quartz, sericite, mica, tourmaline, pyrite, chalcolite, digenite, hematite, rutile
125	0.48		quartz, sericite, mica, tourmaline, pyrite, chalcocite, digenite, hematite, rutile
128	0.34	quartz, muscovite, tourmaline, titanite, chalcopyrite	
132	0.49		
133	0.13		
137	0.23	quartz, pyrite, muscovite, orthoferrosilite	
145	0.38	quartz, pyrite, muscovite	
148	1.07		